Spectral-Efficiency - Illumination Pareto Front for Energy Harvesting Enabled VLC Systems

Amr M. Abdelhady, Osama Amin, Anas Chaaban, Basem Shihada, and Mohamed-Slim Alouini

Abstract

The continuous improvement in optical energy harvesting devices motivates the development of visible light communication systems that utilize such available free energy. In this paper, an outdoor visible light communications (VLC) system is considered where a VLC base station sends data to multiple users that are capable of harvesting optical energy. The proposed VLC system serves multiple users using time division multiple access (TDMA) with unequal time and power allocation, which are allocated to achieve the system communications and illumination objectives. In an outdoor setup, the system lighting objective is to maximize the average illumination flux, while the communication design objective is to maximize the spectral efficiency (SE). A multiobjective optimization problem is formulated to obtain the Pareto front of the SE-illumination region. To this end, the marginal optimization problems are solved first using low complexity algorithms. Then, based on the proposed algorithms, a Karush-Kuhn-Tucker-based algorithm is developed to obtain an inner bound of the Pareto front for the SE-illumination tradeoff. The inner bound for the Pareto-front is shown to be close to the optimal Pareto-frontier via several simulation scenarios for different system parameters.

Index Terms

Visible light communication, spectral efficiency, illumination, energy harvesting, Pareto front, multiobjective optimization, outdoor communication, mass gathering events.

A. M. Abdelhady, O. Amin, B. Shihada and M.-S. Alouini are with the Computer Electrical, and Mathematical Science and Engineering (CEMSE) Division, King Abdullah University of Science and Technology (KAUST), Thuwal, Makkah Province, Kingdom of Saudi Arabia, E-mail: {amr.abdelhady, osama.amin, basem.shihada, slim.alouini}@kaust.edu.sa.

A. Chaaban is with the University of British Columbia, Okanagan campus, Kelowna, BC, Canada, Email: anas.chaaban@ubc.ca.

The SE optimization part of this work was presented in [1].

I. Introduction

Optical wireless communications (OWC) is a powerful technology that is able to address the spectrum scarcity effectively [2]. It offers different solutions that can meet the exponential increase of wireless communication demand by accessing the infrared, visible and ultraviolet (UV) bands. Free space optical (FSO) communication using infrared laser offers a high speed solution for different applications such as backhaul links. On the other hand, it may suffer from some impairments such as pointing errors, scattering, turbulence and terminal swing. UV or optical scattering communication relaxes the line-of-sight (LoS) requirement in FSO by using wide field-of-view (FOV) receivers and exploiting scattering, while benefiting from the fact that background UV noise from solar radiation is negligible at the ground level. However, the transmitted power should be monitored carefully to satisfy safety requirements.

Among the optical spectrum, the visible light range receives particular interest due to its widespread usage for illumination especially after using light emitting diodes (LEDs) that are capable to support both illumination and communication services. Visible light communications (VLC) has several advantages over radio frequency (RF) communications, which encourages considering it for next generation wireless networks [3]–[6]. For instance, VLC uses the wide visible light spectrum that extends from a wavelength of 380 nm to 750 nm. Additionally, VLC can benefit from existing infrastructure which makes it cheaper than setting up new RF networks. Furthermore, VLC offers a ubiquitous indoor and outdoor coverage wherever the illumination service is required. Most research on VLC focused on indoor applications [3], [7]–[12], where a specific illumination level is required. On the other hand, outdoor VLC has not received much attention except for vehicular applications [13]–[15].

Recently, light energy harvesting-enabled communications systems have gained lots of interest. A multitiude of such systems have been investigated in the literature [1], [16]–[23]. In [16], [17] a hybrid VLC/RF relaying communications system with light energy harvesting support was studied for single and multiple transceivers. In [1], [18], resource allocation problems with the aim of spectral efficiency (SE) maximization for the downlink of a single cell energy harvesting enabled VLC system were considered. By an experimental demonstration, Liu *et al.* proposed a solar cell based VLC receiver that is capable of handling both energy harvesting and data decoding [19]. In that work, the developed system was evaluated based on error probability and generated voltage versus illuminance. As the interest in energy harvesting enabled VLC systems

increased, Diamantoulakis *et al.* coined the "SLIPT" term and proposed different strategies for the system operation [20], [24].

In this paper, we shed light on one of the promising outdoor VLC applications, namely, serving mass gathering night events, e.g., social or sports events, where a high degree of illumination is required. Using VLC in such circumstances is encouraged for many reasons. First, the absence of sunlight interference allows for developing a robust communication link. Additionally, the high illumination intensity requirement implies the availability of a strong signal that can serve a large number of users with high data rates. Moreover, using VLC reduces infrastructure costs as there is no need to set up a new wireless network or use mobile base stations, thereby reducing interference and sparing the RF spectrum. Finally, the high illumination intensity requirement makes energy harvesting promising and viable. Unlike indoor VLC systems which has tight equality temporal illumination requirements, in outdoor setups we are interested in illumination maximization under powerlimited power budget constraitns with some tolerance in illumination temporal variability. Throughout this paper, we study the problem of allocating the resources of a VLC system based on TDMA scheme to maximize the system SE and illumination performance whilst satisfying quality-of-service (QoS) requirements. The proposed system supports both illumination and communications services, we define QoS in terms of the harvested energy and edge users' rate. To study the tradeoff betweem SE and illumination performance, we consider a multi-objective optimization problem (MOOP) to obtain the best tradeoff curve (Pareto front) between SE and illumination subject to QoS constraints. To this end, we start by solving the marginal problems, i.e., maximizing the SE and the illumination, by deriving the necessary optimality conditions which are then utilized in proposing low complexity sub-optimal algorithms. Then, we derive the necessary optimality conditions for the MOOP that lead to the optimal SE-illumination Pareto front and propose a low complexity resource allocation algorithm based on the proposed algorithms for the marginal problems. The proposed algorithms can be implemented in the controller of the VLC base station, where they should be executed every coherence time. Finally, we present extensive simulations that confirm our proposed algorithms' capabilities compared with the optimal solution and show the average SE and illumination performance with respect to different system parameters. Furthermore, we assess the flickering performance of the proposed optimization using our new proposed flickering metric.

The rest of the paper is organized as follows. Section II defines the system model for an outdoor

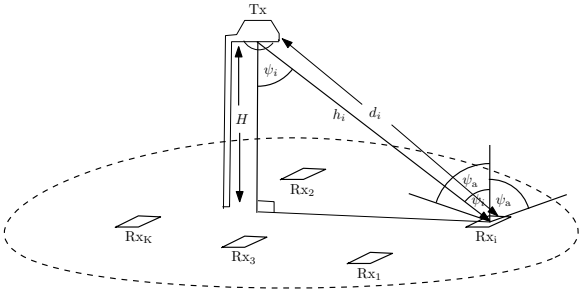

Fig. 1: System Model

VLC system and different design metrics. Sections III and IV study the marginal optimization problems of the MOOP. Then, the Pareto front solution is investigated in Section V. Finally, Section VI presents comprehensive numerical results before concluding the paper in Section VII.

II. System Model

Consider an outdoor VLC system consisting of a powerful transmitter serving K users using dynamic TDMA with a modulation bandwidth of B_{v} Hz. All users have visible light energy harvesting capabilities as long as they are in the coverage area. The received signal by the i-th user is modeled as

$$y_i = h_i s_i + n_i, \tag{1}$$

where s_i is the current used to transmit a symbol to the i-th user, h_i represents the VLC channel gain between the transmitter and the i-th receiver, and n_i is a zero mean additive white Gaussian noise with variance σ_n^2. The non-negativity of s_i is necessary for the operation of VLC systems, since the driving current of an LED has to be positive.

The transmission frame duration T seconds is divided between users such that user i is allotted $\tau_i T$ seconds during each transmission frame, where $\sum_{i=1}^{K} \tau_i = 1$. Due to practical switching limitations, it is required that $\tau_i \geq \tau_{\min}\ \forall i$. Due to operational specifications, the average power at the transmitter is desired to be P_{D}, i.e., $\sum_{i=1}^{K} \tau_i \mathbb{E}\{s_i^2\} = P_{\text{D}}$. In this work, we adopt the followed model in [25] where the channel gain h_i between the transmitter and receiver i depends solely on the relative position of the receiver with respect to the transmitter, and is given by:

$$h_i = \eta_{\text{eo}} \frac{(m+1) A_{\text{PD}} R_{\text{PD}}}{2\pi d_i^2} \cos^{m+1}(\psi_i) \frac{n^2}{\sin^2(\psi_{\text{a}})} \text{rect}\left(\frac{\psi_i}{\psi_{\text{a}}}\right), \tag{2}$$

where $m = -\ln 2/\ln(\cos(\phi_{\rm a}))$ is the Lambertian order, $\phi_{\rm a}$ is the semi-angle at half-power of the light source emission pattern, $A_{\rm PD}$ is the effective photo-detector area, $R_{\rm PD}$ is the photo-detector responsivity, d_i is the distance between the transmitter and user i, ψ_i is the angle between the incident light ray and the normal to the photo-detector plane as depicted in Fig. 1, n is the refractive index of the concentrator, $\psi_{\rm a}$ is the field of view of the user's receiver concentrator, and rect(x) is the rectangular function defined as rect$(x) = 1$ if $|x| \leq 1$, and 0 otherwise. We assume perfect knowledge of h_i $\forall i$ at the transmitter via a feedback with the receivers. This assumption is reasonable in a quasi-static channel where h_i maintains the same value throughout a transmission block, and changes in between blocks due to change of location. The electrical to optical conversion efficiency $(\eta_{\rm eo})$ is assumed to be one, and the optical to electrical conversion efficiency is directly proportional to $R_{\rm PD}$, and hence s_i can also be interpreted as optical intensity.

In this work we express the overall system SE using the achievable rate for VLC systems presented in [26] with $s_i \sim$ Exponential$(1/x_i)$ as

$$\eta_{\rm SE}(\mathbf{x}, \boldsymbol{\tau}) = \frac{1}{2}\sum_{i=1}^{K} \tau_i \log_2\left(1 + \gamma_i x_i^2\right), \tag{3}$$

where $\mathbf{x} = (x_1, x_2, \ldots, x_K)$ is the average current allocation vector, i.e., $x_i = \mathbb{E}\{s_i\}$, $\boldsymbol{\tau} = (\tau_1, \tau_2, \ldots, \tau_K)$ is the time fraction allocation vector, and γ_i is the i-th user channel-to-noise ratio defined as $\gamma_i = \frac{e}{2\pi} h_i^2/\sigma_n^2$.

Since the average illumination intensity of the transmitter is proportional to the average LED excitation current intensity [27, Ch. 1], we use the latter quantity as a measure for illumination which can be expressed as follows

$$\mathcal{I}(\mathbf{x}, \boldsymbol{\tau}) = \sum_{i=1}^{K} \tau_i x_i. \tag{4}$$

The average harvested power by the $i-$th user is given by $P_{{\rm h},i} = 0.75 V_{\rm T} \sum_{j=1}^{K} \tau_j h_i x_j \ln\left(1 + \frac{h_i x_j}{I_{\rm o}}\right)$, where $V_{\rm T}$ is the thermal voltage (mVolt) and $I_{\rm o}$ is the photo-detector dark saturation current [16].

The system QoS requirements are represented as a worst-case user rate requirement and an energy harvesting requirement per user. The former is imposed to ensure minimum rate for all users when they experience the same channel as the furthest one, and are given the minimum time transmission duration. The latter guarantees that all users cover a portion of their circuits energy consumption through harvesting. Moreover, eye-safety requirements are enforced by keeping the maximum illuminance (right beneath the transmitter) $L_{\max} = \sum_{i=1}^{K} \eta_\phi \tau_i x_i \frac{m+1}{2\pi d_{\min}^2}$ below a certain

threshold $L_{\rm th}$, where η_ϕ represents the ratio between the LED luminous flux and its excitation current, and $d_{\min}$ is the minimum possible distance between the transmitter and the users.

The previously mentioned metrics (SE and illumination intensity) evaluate the outdoor VLC system performance in terms of communication and lighting. It is desirable for outdoor VLC setups to maximize these metrics. To solve the MOOP in a tractable way, we study first the marginal optimization problems, then we solve the MOOP using the proposed solutions for the marginal problems. This procedure is detailed in the following sections.

III. Communications-oriented operation

In this section, we study the communications service perspective of the proposed VLC system, where the emphasis is on maximizing the SE whilst satisfying the imposed requirements in terms of energy harvesting, individual user minimum rate, and eye-safety requirements.

A. SE Maximization Problem Formulation

The communications-driven system operation is governed by the following problem

$$\begin{aligned}
\mathbf{(P1)} \quad \max_{\mathbf{x},\boldsymbol{\tau}} \quad & \eta_{\rm SE}\left(\mathbf{x},\boldsymbol{\tau}\right) \\
\text{subject to} \quad & \mathrm{C1}: \sum\nolimits_{i=1}^{K} \tau_i x_i^2 = P_{\rm M}, \;\; \mathrm{C2}: \sum\nolimits_{i=1}^{K} \tau_i = 1, \;\; \mathrm{C3}: P_{{\rm h},i} \geq \beta P_{\rm cr} \tau_i \quad \forall i, \\
& \mathrm{C4}: \tau_i \geq \tau_{\min} \;\; \forall i, \qquad \mathrm{C5}: R_{{\rm wc},i} \geq R_{\rm th} \, \forall i,
\end{aligned}$$

where $P_{\rm M} = \min\left(P_{\rm D}, \left(\frac{L_{\rm th}}{\eta_\phi \bar{h}}\right)^2\right)$, $P_{\rm D}$ represents desired system average operation power, $\bar{h} = \frac{m+1}{2\pi d_{\min}^2}$, $R_{{\rm wc},i} = \frac{B_{\rm v}\tau_{\min}}{2}\log_2\left(1+\gamma_{\min}x_i^2\right)$, where $\gamma_{\min} = \min\limits_i \gamma_i$, and $P_{\rm cr}$ represent the receiver circuits power usage. C1 sets the system average power at the desired level unless it violates eye-safety requirements. Eye-safety is guaranteed by enforcing $L_{\max} \leq L_{\rm U} = \sqrt{\sum_{i=1}^{K}\tau_i x_i^2}\sqrt{\sum_{i=1}^{K}\tau_i} \leq L_{\rm th}$, which necessitates that $\sum_{i=1}^{K}\tau_i x_i^2 \leq \left(\frac{L_{\rm th}}{\eta_\phi \bar{h}}\right)^2$. C2 denotes the time allocation constraint, C3 is the energy harvesting constraint, C4 states the minimum time slot according to hardware switching limitations, and C5 guarantees per-user worst-case rate.

Due to the inherent complexity of C3, we consider a tighter constraint represented by $\tau_i \leq \frac{\bar{E}_{{\rm h},i}}{\beta P_{\rm cr}} \triangleq \tau_{{\max},i}$, where $\bar{E}_{{\rm h},i} = 0.75 V_{\rm T} \sum\limits_{j=1}^{K} \sqrt{\tau_{j,{\rm h}}^* z_{j,{\rm h}}^*} h_i \ln\left(1+\frac{h_i}{I_{\rm o}}\sqrt{\frac{z_{j,{\rm h}}^*}{\tau_{j,{\rm h}}^*}}\right)$, $\{z_{j,{\rm h}}^*\}_{j=1}^K$ and $\{\tau_{j,{\rm h}}^*\}_{j=1}^K$ are the optimal solutions of $\mathbf{(P0)}$ shown in Appendix A. Moreover, C5 can be written equivalently as $x_i \geq \sqrt{\left(2^{2R_{\rm th}/(B_{\rm v}\tau_{\min})}-1\right)/\gamma_{\min}} \triangleq x_{\min}$. Then, we note that $\mathbf{(P1)}$ is not a convex optimization

problem since $\eta_{\mathrm{SE}}(\mathbf{x}, \boldsymbol{\tau})$ is not concave in $\mathbf{x}$ and $\boldsymbol{\tau}$. Therefore, to convexify the problem, we reformulate $\mathbf{(P1)}$ using the transformation $z_i = \tau_i x_i^2$ to obtain

$$\begin{aligned}
\mathbf{(\tilde{P}1)} \quad & \max_{\mathbf{z},\boldsymbol{\tau}} && \tilde{\eta}_{\mathrm{SE}}(\mathbf{z}, \boldsymbol{\tau}) = \sum_{i=1}^{K} \tau_i \ln\left(1 + \frac{\gamma_i z_i}{\tau_i}\right) \\
& \text{subject to} && \mathrm{C1}: \sum\nolimits_{i=1}^{K} z_i = P_{\mathrm{M}}, \quad \mathrm{C2},\ \mathrm{C4} \\
& && \mathrm{C3}: \tau_i \leq \tau_{\max,i}\ \forall i, \qquad \mathrm{C5}: z_i \geq z_{\min}\ \forall i,
\end{aligned}$$

where $\mathbf{z} = (z_1, z_2, \ldots, z_K)$ is the power allocation vector, and $z_{\min} = \tau_{\min} x_{\min}^2$. One can show that $\tilde{\eta}_{\mathrm{SE}}(\mathbf{z}, \boldsymbol{\tau})$ is a jointly concave function in both $\mathbf{z}$ and $\boldsymbol{\tau}$ using the perspective transform of $\ln(1 + \gamma_i z_i)$ which is a concave function in $\mathbf{z}$ [28]. In addition, all the constraints are affine, thus, $\mathbf{(\tilde{P}1)}$ is a convex optimization problem and the Karush-–Kuhn-–Tucker (KKT) conditions guarantee global optimality [28].

B. Proposed Solution Details

In what follows, we present the KKT system of equations associated with $\mathbf{(\tilde{P}1)}$ and propose a low-complexity approach to solve it as follows:

The Lagrangian of $\mathbf{(\tilde{P}1)}$ can be formulated as

$$\begin{aligned}
\mathcal{L} = & \sum_{i=1}^{K} \tau_i \ln\left(1 + \frac{\gamma_i z_i}{\tau_i}\right) + \mu\left(P_{\mathrm{M}} - \sum_{i=1}^{K} z_i\right) + \sum_{i=1}^{K} o_i (z_i - z_{\min}) + \sum_{i=1}^{K} \nu_i (\tau_{\max,i} - \tau_i) \\
& + \lambda\left(1 - \sum_{i=1}^{K} \tau_i\right) + \sum_{i=1}^{K} \kappa_i (\tau_i - \tau_{\min}).
\end{aligned} \tag{5}$$

The KKT conditions of $\mathbf{(\tilde{P}1)}$ can be summarized as

$$\frac{\partial \mathcal{L}}{\partial z_i} = \frac{\gamma_i}{1 + \gamma_i z_i/\tau_i} - \mu + o_i = 0, \tag{6}$$

$$\frac{\partial \mathcal{L}}{\partial \tau_i} = \ln\left(1 + \frac{\gamma_i z_i}{\tau_i}\right) - \frac{\gamma_i z_i}{\tau_i + \gamma_i z_i} - \nu_i - \lambda + \kappa_i = 0, \tag{7}$$

$$o_i (z_i - z_{\min}) = \nu_i (\tau_i - \tau_{\max,i}) = \kappa_i (\tau_i - \tau_{\min}) = 0, \tag{8}$$

$$o_i \geq 0, \quad \nu_i \geq 0, \quad \kappa_i \geq 0 \tag{9}$$

$\forall i$ in addition to the conditions $\mathrm{C1}-\mathrm{C5}$. The convexity of $\mathbf{(\tilde{P}1)}$ implies that strict complementary slackness applies [28], such that $o_i = 0$ if and only if (iff) $z_i > z_{\min}$ and $o_i > 0$ iff $z_i = z_{\min}$ $\forall i$. Similarly, $\kappa_i = 0$ iff $\tau_i > \tau_{\min}$, $\kappa_i > 0$ iff $\tau_i = \tau_{\min}$, $\nu_i = 0$ iff $\tau_i < \tau_{\max,i}$, and $\nu_i > 0$ iff $\tau_i = \tau_{\max,i}$, $\forall i$.

TABLE I: Inequality constraints multipliers configurations for $(\tilde{\mathbf{P1}})$. The optimal (τ_i, z_i) pair is indicated below each case.

		$o_i = 0$		$o_i \neq 0$	
$\nu_i = 0$	$\kappa_i = 0$	**Case 1** (τ_i^*, z_i^*)	$\frac{z_i^*}{\tau_i^*} = \frac{1}{\mu} - \frac{1}{\gamma_i}$ $\ln\left[\frac{\gamma_i}{\mu}\right] - 1 + \frac{\mu}{\gamma_i} = \lambda$	**Case 4** $(\tau_i^*, z_{\min})$	$\frac{z_{\min}}{\tau_i^*} = \frac{1}{\mu - o_i} - \frac{1}{\gamma_i}$ $\ln\left[\frac{\gamma_i}{\mu - o_i}\right] + \frac{\mu - \gamma_i - o_i}{\gamma_i} = \lambda$
	$\kappa_i \neq 0$	**Case 3** $(\tau_{\min}, z_i^*)$	$\frac{z_i^*}{\tau_{\min}} = \frac{1}{\mu} - \frac{1}{\gamma_i}$ $\ln\left[\frac{\gamma_i}{\mu}\right] - 1 + \frac{\mu}{\gamma_i} + \kappa_i = \lambda$	**Case 5** $(\tau_{\min}, z_{\min})$	$\frac{z_{\min}}{\tau_{\min}} = \frac{1}{\mu - o_i} - \frac{1}{\gamma_i}$ $\ln\left[\frac{\gamma_i}{\mu - o_i}\right] + \frac{\mu - \gamma_i - o_i}{\gamma_i} + \kappa_i = \lambda$
$\nu_i \neq 0$	$\kappa_i = 0$	**Case 2** $(\tau_{\max,i}, z_i^*)$	$\frac{z_i^*}{\tau_{\max,i}} = \frac{1}{\mu} - \frac{1}{\gamma_i}$ $\ln\left[\frac{\gamma_i}{\mu}\right] - 1 + \frac{\mu}{\gamma_i} - \nu_i = \lambda$	**Case 6** $(\tau_{\max,i}, z_{\min})$	$\frac{z_{\min}}{\tau_{\max,i}} = \frac{1}{\mu - o_i} - \frac{1}{\gamma_i}$ $\ln\left[\frac{\gamma_i}{\mu - o_i}\right] + \frac{\mu - \gamma_i - o_i}{\gamma_i} - \nu_i = \lambda$

We assume without loss of generality that $\gamma_1 \geq \gamma_2 \geq \cdots \geq \gamma_K$, which implies that $\tau_{\max,1} \geq \tau_{\max,2} \geq \cdots \geq \tau_{\max,K}$. For a given user i, we have many possibilities in terms of the active constraints associated with ν_i, o_i and κ_i (corresponding to zero or nonzero values of $\emptyset_i, \kappa_i$, and ν_i), which results in numerous possible KKT stationarity cases that are summarized in Table I, where τ_i^* and z_i^* denote the optimal values of τ_i and z_i, respectively. Hence, solving the resource allocation problem turns out to be of exponential complexity in terms of K since we will need to try different combinations of the 6 Cases listed in Table I for each user. Therefore, it is desirable to develop low complexity algorithms with performance close to the optimal solution.

In order to reduce the complexity, we make use of the positive monotonicity characteristics of the objective function in $\boldsymbol{\tau}$ and $\boldsymbol{z}$ (cf. Appendix B) and limit our space of solutions to the following structure:

$$\mathbf{z} = \left[z_1^*, .., z_j^*, z_{\min}, .., z_{\min}\right], \quad (10) \qquad \boldsymbol{\tau} = \left[\tau_{\max,1}, .., \tau_{\max,f-1}, \tau_f^*, .., \tau_\ell^*, \tau_{\min}, .., \tau_{\min}\right], \quad (11)$$

where $z_i^* > z_{\min}$ for $i \leq j$ and $\tau_{\max,f-1} > \tau_i^* > \tau_{\min}$ for $f \leq i \leq \ell$ with N_τ unknown time allocation variables, where $N_\tau = \ell - f + 1$. Now, we consider the proposed solution structure and different cases in Table I to allocate the available resources. First, one can easily show that there are no more than two users can fall into Case 1. Then, we need to check different possibilities that meet the aforementioned criteria to find the feasible solution with the best performance. To scan all possibilities, we consider two scenarios $N_\tau = 1$ and $N_\tau > 1$ as follows:

Scenario A: If $N_\tau = 1$, then $f = \ell$ and τ_ℓ^* is obtained from C2 as $\tau_\ell^* = 1 - \sum_{i=1}^{f-1} \tau_{\max,i} - \tau_{\min}(K - \ell)$. To obtain z_i^* for $i \leq j$, we compute it using the corresponding time allocation as $z_i^* = \tau_i \left(\frac{1}{\mu} - \frac{1}{\gamma_i}\right)$, which captures Cases 1, 2 and 3 in Table I. As for μ, it is obtained using C1

Algorithm I-A

for $\ell = KS + (K-1)(1-S), ..., 2, 1$
  $t \leftarrow \sum_{i=1}^{\ell-1} \tau_{\max,i} + (K-\ell)\,\tau_{\min} S + (1-S)\sum_{i=\ell+1}^{K} \tau_{\max,i}$
  if $t < 1$ and $\tau_{\min} < 1 - t < \tau_{\max,\ell}$
    $\tau_\ell \leftarrow 1 - t$, $\tau_i \leftarrow \tau_{\max,i}$, $\forall i \leq \ell - 1$ and $\tau_i \leftarrow \tau_{\min} S + (1-S)\tau_{\max,i}$, $\forall i \geq \ell + 1$
    for $j = K, K-1, \ldots, 1$
      $z_i \leftarrow z_{\min}$, $\forall i > j$
      if $\mathcal{A}$=0
        $z_i \leftarrow \frac{\Gamma_i^2 \tau_i^*}{4\mu^2}, \forall i \leq j$ with μ obtained from (56).
      else
        $z_i \leftarrow \tau_i \left(1/\mu - 1/\gamma_i\right) \quad \forall i \leq j$ with μ obtained from (12).
      end if
      Execute Algorithm I-KKT
      $j \leftarrow j - 1$
    end for
  end if
end for

as

$$\mu = \frac{\sum_{i=1}^{j} \tau_i}{\sum_{i=1}^{j} \frac{\tau_i}{\gamma_i} + P_{\mathrm{M}} - (K-j)\, z_{\min}}. \tag{12}$$

It remains to specify j and ℓ. To do this, we search for $j \in \{1, \ldots, K\}$ and $\ell \in \{1, \ldots, K\}$ using Algorithm I-A[1] and check if the KKT conditions are satisfied using Algorithm I-KKT.

Scenario B: If $N_\tau > 1$, then the proposed solution structure and Case 1 condition impose $j \leq f + 1$. To handle this scenario, we divide the j domain into three sub-scenarios given by $j = f$, $j = f + 1$ and $j < f$. Before considering the different sub-scenarios, we define U_x as the set of user indices belonging to Case x in Table I.

[1]The proposed algorithms are developed to deal with both SE maximization and MOOP by using the parameter $\mathcal{A}$ that takes either 1 or 0 values, respectively, to select the optimization problem.

Algorithm I-KKT

if $\mathbf{z}$ and $\boldsymbol{\tau}$ are feasible, and $\tilde{\eta}_{\mathrm{SE}}(\mathbf{z}, \boldsymbol{\tau}) \geq \eta_{\mathrm{SE}}^{\max}$
  $\mathbf{z}^* \leftarrow \mathbf{z}$, $\boldsymbol{\tau}^* \leftarrow \boldsymbol{\tau}, \eta_{\mathrm{SE}}^{\max} \leftarrow \tilde{\eta}_{\mathrm{SE}}(\mathbf{z}, \boldsymbol{\tau})$
end if
if $\mathcal{A}$=0
  Compute o_i, κ_i, and ν_i using (46) and (47) $\forall i$
else
  Compute o_i, κ_i, and ν_i using (6) and (7) $\forall i$
end if
if KKT conditions are satisfied
  $\mathbf{z}^* \leftarrow \mathbf{z}$, $\boldsymbol{\tau}^* \leftarrow \boldsymbol{\tau}$, **Terminate.**
end if

Scenario B.i: For $j = f$, z_i^* follows Cases 1 and 2 in Table I for $i \leq j$ and is expressed as

$$z_i^* = \begin{cases} \tau_{\max,i}\left(\frac{1}{\mu} - \frac{1}{\gamma_i}\right) \triangleq f_i(\mu), & \forall i \in U_2 \\ \tau_i^*\left(\frac{1}{\mu} - \frac{1}{\gamma_i}\right), & \forall i \in U_1, \end{cases} \tag{13}$$

where $U_2 \triangleq \{1, \ldots, j-1\}$ and $U_1 \triangleq \{j\}$. As for $i \geq j+1$, $z_i = z_{\min}$ according to the proposed structure in (10). On the other hand, τ_i^* is expressed as

$$\tau_i^* = z_{\min}\gamma_i\left(\frac{1}{r_i} - 1\right)^{-1}, \ \forall i \in U_4, \tag{14}$$

where $U_4 \triangleq \{j+1, \ldots, \ell\}$ and $r_i = \frac{\mu - o_i}{\gamma_i}$, while $\tau_i = \tau_{\min}$ for $\ell + 1 \leq i \leq K$.

To evaluate z_i^* from (13) and τ_i^* from (14), we need to find μ and $o_i \, \forall i \in U_4$. Thus, we first rewrite the second equation presented under Case 4 in Table I in terms of r_i obtaining

$$r_i = -\mathcal{W}_0\left(-e^{-(\lambda+1)}\right), \tag{15}$$

where $\mathcal{W}_0(.)$ is the Lambert function [29]. This relation can proved as follows:
To solve $-\ln(r_i) - (1 - r_i) - \lambda = 0$, we rewrite it equivalently as $-\ln(r_i e^{-r_i}) = \lambda + 1$, which can be simplified to $-r_i e^{-r_i} = -e^{-(\lambda+1)}$. Then, by computing LambertW function to both sides of the previous equation we get $-r_i = \mathcal{W}\left(-e^{-(\lambda+1)}\right)$. Since $-r_i \geq -1$ then $r_i = -\mathcal{W}_0\left(-e^{-(\lambda+1)}\right)$. Thus, τ_i^* in (14) can be rewritten in terms of λ as

$$\tau_i^* = z_{\min}\gamma_i\left(\frac{1}{-\mathcal{W}_0\left(-e^{-(\lambda+1)}\right)} - 1\right)^{-1} \triangleq g_i(\lambda), \ \forall i \in U_4. \tag{16}$$

In addition, τ_j^* can be expressed in terms of λ using C2 as,

$$\tau_j^* = 1 - \sum\nolimits_{i\in U_4} g_i(\lambda) - \sum\nolimits_{i=1}^{f-1} \tau_{\max,i} - (K-\ell)\,\tau_{\min}. \tag{17}$$

Since user j follows Case 1, then we can obtain μ by solving Case 1 second equation at $i=j$ obtaining $\mu = -\gamma_j \mathcal{W}_0\left(-e^{-(\lambda+1)}\right)$. (18)

Then, we use C1 and substitute (16)–(18) in (13) obtaining the following equation in λ

$$G(\lambda) = \left(1 - \sum\nolimits_{i=1}^{f-1} \tau_{\max,i} - (K-\ell)\,\tau_{\min} - \sum\nolimits_{i\in U_4} g_i(\lambda)\right)\left(\frac{1}{-\gamma_j \mathcal{W}_0\left(-e^{-(\lambda+1)}\right)} - \frac{1}{\gamma_j}\right) + \sum\nolimits_{i\in U_2} f_i\left(-\gamma_j \mathcal{W}_0\left(-e^{-(\lambda+1)}\right)\right) = P_{\mathrm{M}} - (K-j)\,z_{\min}. \tag{19}$$

The solution of (19) can be obtained by using the bisection numerical method thanks to the monotonic behavior of $G(\lambda)$, which admits a unique solution (cf. Appendix C). By backward substitution, we can get all the unknown primal variables, and then the dual variables can be calculated using (6) and (7). This is illustrated in lines 13–15,19,29 in Algorithm I-B.

Scenario B.ii: For $j = f+1$, we have $U_2 \triangleq \{1,\ldots,j-2\}$, $U_1 \triangleq \{j-1, j\}$ and $U_4 \triangleq \{j+1,\ldots,\ell\}$. $z_i^*, \forall i \in U_1$ or U_2 is evaluated from (13) and $\tau_i^*, \forall i \in U_4$ is evaluated from (16). Similar to our approach in Scenario B.i, we need to know μ and λ to compute z_i^* and τ_i^*. For this purpose, we consider the two users in U_1 and use the second equation of Case 1 in Table I for both users to express μ as $\ln\left(\frac{\gamma_j}{\gamma_{j-1}}\right) / \left(\frac{1}{\gamma_{j-1}} - \frac{1}{\gamma_j}\right)$. (20)

Moreover, we evaluate the same equation for user j to express λ as $\ln\left(\frac{\gamma_j}{\mu}\right) - 1 + \frac{\mu}{\gamma_j}$. (21)

Now, we substitute (13) and (21) in C1 to obtain τ_j^* and τ_{j-1}^* that can be computed as

$$\begin{bmatrix} \tau_j^* \\ \tau_{j-1}^* \end{bmatrix} = \begin{bmatrix} (1/\mu - 1/\gamma_j) & (1/\mu - 1/\gamma_{j-1}) \\ 1 & 1 \end{bmatrix}^{-1} \begin{bmatrix} P_{\mathrm{M}} - z_{\min}(K-j) - \sum_{i\in U_2} z_i^* \\ 1 - \tau_{\min}(K-\ell) - \sum_{i\in U_4} \tau_{\max,i} \end{bmatrix}. \tag{22}$$

Finally, the dual variables can be computed from (6), (7) as shown in Algorithm I-KKT in lines 5 and 7.

Scenario B.iii: For $j < f$, we have $U_1 \triangleq \emptyset$, $U_2 \triangleq \{1,\ldots,j\}$ and $U_4 \triangleq \{j+1,\ldots,\ell\}$. $z_i^*, \forall i \in U_2$ is evaluated from (13) where μ is computed from C1 as

$$\mu = \frac{\sum_{i\in U_2} \tau_{\max,i}}{\sum_{i\in U_2} \frac{\tau_{\max,i}}{\gamma_i} + P_{\mathrm{M}} - (K-j)\,z_{\min}}. \tag{23}$$

As for $\tau_i^*, \forall i \in U_4$, it is evaluated from (16), where λ is found from C2. Afterwards, all unknown $\boldsymbol{\tau}$ variables are obtained. We then calculate the rest of dual variables using (6) and (7). This is illustrated in lines 5 and 7 in Algorithm I-KKT.

Algorithm I-B

for $\ell = \{KS + (K-1)(1-S)(1-\mathcal{A}), \ldots, N_\tau + 1, N_\tau\}$
  $t \leftarrow \sum_{i=1}^{\ell - N_\tau} \tau_{\max,i} + (K-\ell)\,\tau_{\min} S + (1-S)\sum_{i=\ell+1}^{K} \tau_{\max,i}$
  $U_4 \leftarrow \{\ell + 1, \ldots, K\}$
  if $t < 1$ and $(K-\ell)\,\tau_{\min} S + (1-S)\sum_{i=\ell+1}^{K} \tau_{\max,i} < 1 - t < \sum_{i=\ell-N_\tau+1}^{\ell} \tau_{\max,i}$
    $\tau_i \leftarrow \tau_{\max,i}$, $\forall i \leq \ell - 1$ and $\tau_i \leftarrow \tau_{\min} S + \tau_{\max,i}(1-S)$, $\forall i \geq \ell + 1$
    for $j = \ell - N_\tau + 1 + \mathcal{A}, \ldots, 1$
      $z_i \leftarrow z_{\min}$, $\forall i > j$
      if $\mathcal{A} = 1$
        if $j = \ell - N_\tau + 2$
          $U_2 \leftarrow \{1, \ldots, j-2\}$
          Compute μ from (20), Then **get** λ from (21), τ_j, τ_{j-1} from (22), z_j, z_{j+1} from (13)
        else if $j = \ell - N_\tau + 1$
          $U_2 \leftarrow \{1, \ldots, j-1\}$, **Solve** (18) for μ and (19) for λ
          Compute z_j and τ_j from (13) and (17), respectively
        else
          $U_2 \leftarrow \{1, \ldots, j\}$, **Solve** (17) for λ with $\tau_j = 0$, **Compute** μ from (23)
        end if
        Compute z_i from (13) $\forall i \in U_2$, τ_i from (16) $\forall i \in U_4$.
      else $\quad \%\mathcal{A} = 0$
        if $j = \ell - N_\tau + 1$
          $U_2 \leftarrow \{1, \ldots, j-1\}$, **Compute** λ from (48), then **Compute** μ from (49)
          Compute z_j and τ_j from (52) and (53), respectively.
        else
          Compute λ from (54), μ from (55)
        end if
        Compute τ_i from (51) $\forall i \in U_4$, z_i from (50) $\forall i \in U_2$
      end if
      Execute Algorithm I-KKT
    end for
  end if
end for

In summary, Algorithm I proceeds through three composite stages. The first stage scans values of N_τ that is initially set to 1 and is incremented by one after each failed iteration (when KKT conditions are not satisfied). In the second stage, we look over all possible f values which yields a feasible time allocation (lines 1–5 in Algorithms I-A and I-B). For every feasible f value, the third stage loops over the possible configurations for $\mathbf{z}$ variables (j values). For each computed solution, the primal and dual variables are calculated, the solution feasibility is checked and the solution is compared to the best feasible solution found so far $\eta_{\mathrm{SE}}^{\max}$ (lines 6 onwards in Algorithms I-A and I-B). If the current solution has a better objective function value than $\eta_{\mathrm{SE}}^{\max}$, we save the current solution and update $\eta_{\mathrm{SE}}^{\max}$.

Algorithm I : SE optimization / SE-illumination MOOP

1: **Input** $\mathcal{A}, P_{\mathrm{M}}, z_{\min}, \tau_{\min}, \beta, \gamma_i, \tau_{\max,i}\, \forall i \in \{1, .., K\}$ % $\mathcal{A}$=1 or 0 for max SE or MOOP, respectively
2: **Initialize** $N_\tau = 1$
3: **if** $\mathcal{A} = 0$
4: **Compute** $\eta_{\mathrm{SE}}^{\max}, \mathcal{I}_{\max}$ by invoking Algorithm I with $\mathcal{A}$=1, and Algorithm IV respectively.
5: **else**
6: **Initialize** $\eta_{\mathrm{SE}}^{\max} \leftarrow 0$
7: **end if**
8: **for** $S = 1, \ldots, \mathcal{A}$
9: **for** $N_\tau = 1, \ldots, K$
10: **if** $N_\tau = 1$
11: **Execute** Algorithm I-A
12: **else**
13: **Execute** Algorithm I-B
14: **end if**
15: **end for**
16: **end for**

C. Reduced Complexity Algorithms

Throughout this subsection, we present two simpler algorithms than Algorithm I to find a solution that maximizes the SE while meeting the required QoS. As for the complexity of Algorithm I, it depends on number of users, i.e., K. Algorithm I consists of three composite

iterative stages where the worst case complexity of each is $\mathcal{O}(K)$, resulting in an overall complexity of $\mathcal{O}(K^3)$. One way to reduce the complexity is to force N_τ to be 1, which guarantees finding a feasible solution. As a result, the proposed reduced complexity algorithm or ***Algorithm II*** has two composite iterative stages that leads to a complexity of $\mathcal{O}(K^2)$. Algorithm II is realized by modifying line 4 of Algorithm I to be $N_\tau \leq 1$ instead of $N_\tau \leq K$.

We can further reduce the complexity to be $O(K)$ by adopting ***Algorithm III*** to allocate the available resources. In this algorithm, the time budget is poured such that all users at first are allocated the minimum amount of time $\tau_{\min}$, then the remaining budget $(1-K\tau_{\min})$ is distributed iteratively such that users are allocated their time portions in descending order of channel gains, where in the i-th iteration, user i is allocated the minimum between the remaining time budget and the maximum time portion $\tau_{\max,i}$. As for the power, it is assumed to be allocated uniformly among users.

Algorithm III: SE optimization

1: **Input** $\tau_{\min}$, $\tau_{\max,i}$, $\forall i \in \{1,\ldots,K\}$
2: **Initialize** $j = \ell = K$, $n = 1$, where $n \equiv N_\tau$
3: **for** $\ell = K : -1 : 1$
4: $t \leftarrow \sum_{i=1}^{\ell-1} \tau_{\max,i} + (K-\ell)\,\tau_{\min}$
5: **if** $t < 1$ and $\tau_{\min} < 1 - t < \tau_{\max,\ell}$
6: $\tau_i \leftarrow \tau_{\max,i}$, $\forall i \leq \ell - 1$ and $\tau_i \leftarrow \tau_{\min}$, $\forall i \geq \ell + 1$
7: $\tau_\ell \leftarrow 1 - t$, $z_i \leftarrow P_{\mathrm{M}}/K$
8: **end if**
9: **end for**

D. Problem Feasibility

In this subsection, we present the conditions required for the feasibility of the considered optimization problems. By inspecting $\mathrm{C1}-\mathrm{C5}$ it can be shown that the following conditions are necessary and sufficient for having a non-empty feasibility region

$$\min_i \tau_{\max,i} \geq \tau_{\min}, \quad (24) \qquad K\tau_{\min} \leq 1, \quad (25) \quad \sum_{i=1}^{K} \tau_{\max,i} \geq 1, \quad (26) \qquad K z_{\min} \leq P_{\mathrm{M}}. \quad (27)$$

Condition (24) is necessary to maintain the problems feasible from $\mathrm{C3}$ and $\mathrm{C4}$ perspective. Moreover, condition (25) is necessary for problem feasibility considering $\mathrm{C2}$ and $\mathrm{C4}$ constraints.

In addition, it can be deduced that condition (26) is necessary for C2 and C3 constraints and (27) is needed to satisfy C1 and C5.

The aforementioned feasibility condition set can give bounds for K. Specifically, (25) and (27) can provide an upper bound on the number of users ($K \leq \min\left(P_{\mathrm{M}}/z_{\min}, 1/\tau_{\min}\right)$) that can be accommodated given the existing channel conditions and the required data transmission rate. On the other hand, a lower bound on K can be deduced from (26).

IV. Illumination-oriented operation

Unlike the conventional RF systems where the signal amplitude is not of interest, in VLC systems it maps to the luminous intensity of the LED in a linear fashion, which contributes to the illumination quality of service. In this section, we study the illumination service perspective of the proposed VLC system, where the average LED excitation current is maximized whilst keeping individual user rates, eye-safety, and energy harvesting requirements at desired levels. In addition, we propose a metric to assess the photometric flickering effect for the proposed VLC system.

A. Illumination Maximization Problem

We formulate the illumination maximization problem whilst applying the same transformation of variables, $z_i = \tau_i x_i^2 \ \forall i$, on the illumination objective function (4) and the constraints as

$$\mathbf{(\tilde{P}2)} \qquad \max_{\boldsymbol{z},\boldsymbol{\tau}} \quad \sum\nolimits_{i=1}^{K} \sqrt{z_i \tau_i}$$

$$\text{subject to} \quad \mathrm{C1} - \mathrm{C5}.$$

It can be easily proven that $\mathbf{(\tilde{P}2)}$ is a convex optimization problem, as the objective function is the positive weighted sum of concave functions [28]. The function $\sqrt{z_i \tau_i}$ represents the perspective transform of $\sqrt{z_i}$ with respect to τ_i, which confirms the concavity of $\sqrt{z_i \tau_i}$ [28].

The Lagrangian of problem $\mathbf{(\tilde{P}2)}$ can be expressed as

$$\mathcal{L}_{\mathrm{I}} = \sum\nolimits_{i=1}^{K} \sqrt{\tau_i z_i} + \mu \left(P_{\mathrm{M}} - \sum\nolimits_{i=1}^{K} z_i\right) + \sum\nolimits_{i=1}^{K} o_i \left(z_i - z_{\min}\right) + \lambda \left(1 - \sum\nolimits_{i=1}^{K} \tau_i\right)$$
$$+ \sum\nolimits_{i=1}^{K} \nu_i \left(\tau_{i,\max} - \tau_i\right) + \sum\nolimits_{i=1}^{K} \kappa_i \left(\tau_i - \tau_{\min}\right). \tag{28}$$

The KKT conditions of this problem can be summarized as:

$$\frac{\partial \mathcal{L}_{\mathrm{I}}}{\partial z_i} = \frac{1}{2}\sqrt{\frac{\tau_i}{z_i}} - \mu + o_i = 0 \quad \forall i \in \{1, \ldots, K\}, \tag{29}$$

$$\frac{\partial \mathcal{L}_{\mathrm{I}}}{\partial \tau_i} = \frac{1}{4}\frac{1}{(\mu - o_i)} - \nu_i - \lambda + \kappa_i = 0 \quad \forall i \in \{1, \ldots, K\}, \tag{30}$$

TABLE II: Inequality constraints multipliers configurations for $(\tilde{\mathbf{P2}})$. The optimal (τ_i, z_i) pair is indicated below each case.

	$o_i = 0$		$o_i \neq 0$	
$\nu_i = 0$	**Case 1** (τ_i^*, z_i^*)	$\frac{z_i^*}{\tau_i^*} = \frac{1}{4\mu^2}$ and $\frac{1}{4\mu} - \lambda = 0$	**Case 3** $(\tau_i^*, z_{\min})$	$\frac{z_{\min}}{\tau_i^*} = \frac{1}{4(\mu - o_i)^2}$ and $\frac{1}{4(\mu - o_i)} - \lambda = 0$
$\nu_i \neq 0$	**Case 2** $(\tau_{\max,i}, z_i^*)$	$\frac{z_i^*}{\tau_{\max,i}} = \frac{1}{4\mu^2}$ and $\frac{1}{4\mu} - \nu_i - \lambda = 0$	**Case 4** $(\tau_{\max,i}, z_{\min})$	$\frac{z_{\min}}{\tau_{\max,i}} = \frac{1}{4(\mu - o_i)^2}$ and $\frac{1}{4(\mu - o_i)} - \nu_i - \lambda = 0$

in addition to $\mathrm{C1} - \mathrm{C5}$, (9) and (8).

The convexity of problem $(\tilde{\mathbf{P2}})$ implies strict complementary slackness, where $o_i = 0$ iff $z_i > z_{\min}$ and $o_i > 0$ iff $z_i = z_{\min}$ $\forall i$. Similarly, $\kappa_i = 0$ iff $\tau_i > \tau_{\min}$, $\kappa_i > 0$ iff $\tau_i = \tau_{\min}$, $\nu_i = 0$ iff $\tau_i < \tau_{\max,i}$, and $\nu_i > 0$ iff $\tau_i = \tau_{\max,i}$, $\forall i$. To avoid the exponential complexity of solving the KKT system due to presence of inequality constraints, we limit our space of solutions to specific structure(s). In the following, we propose a structure inspired by the impact of different constraints.

To find a good structure for the solution, we first consider $(\tilde{\mathbf{P2}})$ with $\mathrm{C1}$, and $\mathrm{C2}$ only. The solution of the simplified problem reduces to $z_i^* = P_{\mathrm{M}} \tau_i^*$, which can be proven using Cauchy-Shwartz inequality[2]. After adding $\mathrm{C3} - \mathrm{C5}$, we have $\tau_{\min} \leq \tau_i \leq \tau_{\max,i}$, which may violate the proposed structure if $z_{\min} > P_{\mathrm{M}} \min_i \tau_{\max,i}$. One way to find a solution with a close structure to $z_i^* = P_{\mathrm{M}} \tau_i^*$ while satisfying the constraints is to allot the marginal resources to some users, i.e., $\tau_{\max,i}$ and $z_{\min}$, while others should be computed according to the KKT conditions. Consequently, we limit our search space to the following format:

$$\boldsymbol{z}^* = \left[z_1^*, \ldots, z_\ell^*, z_{\min}, \ldots, z_{\min}\right], \qquad (31) \qquad \boldsymbol{\tau}^* = \left[\tau_1^*, \ldots, \tau_j^*, \tau_{\max,j+1}, \ldots, \tau_{\max,K}\right]. \quad (32)$$

Based on the adopted solution structure and the KKT conditions, all possibilities of the associated inequality multipliers are listed in Table II. As for the indices, there are two possible scenarios either $j \leq \ell$ or $j > \ell$ as discussed in the sequel.

Scenario A: when $j \leq \ell$, z_i^* is expressed in terms of τ_i^* for $i \leq j$ according to Case 1 as

$$z_i^* = 4\lambda^2 \tau_i^* \, \forall i \in U_1, \qquad (33)$$

[2]It is worthy to note that uniform allocation solution ($z_i = P_{\mathrm{M}}/K, \tau_i = 1/K \, \forall i$) is one of the solutions that follow this structure.

where $U_1 \triangleq \{1,\dots,j\}$. For $j < i \leq \ell$, z_i^* is found based on Case 2 as

$$z_i^* = 4\lambda^2 \tau_{\max,i} \, \forall i \in U_2, \tag{34}$$

where $U_2 \triangleq \{j+1,\dots,\ell\}$. Now, λ can be found from C1 and C2 as

$$\lambda = \frac{1}{2}\sqrt{\frac{P_{\mathrm{M}} - (K-\ell)\, z_{\min}}{1 - \sum_{i\in U_4} \tau_{\max,i}}}, \tag{35}$$

where $U_4 \triangleq \{\ell+1,\dots,K\}$.

It can be proved that for a given configuration of ℓ and j to be feasible, the following conditions should be met

$$\tau_{\min} \leq \frac{z_{\min}}{4\lambda^2} \leq \min_{i\in U_2} \tau_{\max,i} \quad \text{and} \quad j\frac{z_{\min}}{4\lambda^2} \leq 1 - \sum_{i\in U_4} \tau_{\max,i} - (\ell - j)\frac{z_{\min}}{4\lambda^2} \leq \sum_{i\in U_1} \tau_{\max,i}. \tag{36}$$

For a given feasible choice of ℓ, j, τ_i^* where $i \in U_1$ are selected to satisfy the following conditions

$$\frac{z_{\min}}{4\lambda^2} \leq \tau_i \leq \tau_{\max,i} \, \forall i \in U_1, \sum_{i\in U_1} \tau_i = 1 - \sum_{i\in U_4} \tau_{\max,i} - (\ell - j)\frac{z_{\min}}{4\lambda^2} \tag{37}$$

, then the rest of τ_i^* variables and z_i^* are computed as discussed previously, and the optimality is examined by finding $\nu_i, o_i \, \forall i$ from (29) and (30).

Scenario B: when $j > \ell$, z_i^* can be expressed in terms of τ_i^* $i \leq \ell$ based on Case 1 using (33), where $U_1 \triangleq \{1,\dots,\ell\}$. Also, τ_i^* for $\ell < i \leq j$ can be expressed based on Case 3 as

$$\tau_i^* = \frac{z_i^*}{4\lambda^2} \quad \forall i \in U_3, \tag{38}$$

where $U_3 \triangleq \{\ell+1,\dots,j\}$, and $U_4 \triangleq \{j+1,\dots,K\}$. Consequently, λ can be obtained by solving C1 and C2 as: $\lambda = \frac{1}{2}\sqrt{\left(P_{\mathrm{M}} - (K-j)\, z_{\min}\right) / \left(1 - \sum_{i\in U_4} \tau_{\max,i}\right)}$. (39)

The ℓ, and j configurations feasibility is determined by satisfying the following conditions:

$$\frac{z_{\min}}{4\lambda^2} \leq \min_{i\in U_3} \tau_{\max,i}, \; \tau_{\min} \leq \min_{i\in U_1} \tau_{\max,i} \text{ and } \; \ell \max\left(\frac{z_{\min}}{4\lambda^2}, \tau_{\min}\right) \leq 1 - \sum_{i\in U_4\cup U_3} \tau_{\max,i} \leq \sum_{i\in U_1} \tau_{\max,i}. \tag{40}$$

After asserting the configuration feasibility, τ_i^* where $i \in U_1$ are allocated any arbitrary allocation that satisfies the following conditions

$$\max\left(\frac{z_{\min}}{4\lambda^2}, \tau_{\min}\right) \leq \tau_i \leq \tau_{\max,i} \, \forall i \in U_1, \sum_{i\in U_1} \tau_i = 1 - \sum_{i\in U_3\cup U_4} \tau_{\max,i} \tag{41}$$

Then the rest of z_i^* and τ_i^* variables are calculated as per the previous discussion. Finally, the solution optimality is checked by calculating the dual variables from (29) and (30).

Both scenarios are implemented in Algorithm IV, where we scan at most $(K-1)^2$ different ℓ and j configurations. For each configuration, the feasibility is tested and all unknown primal

Algorithm IV: Illumination optimization

Input $P_{\mathrm{M}}, \tau_{\min}$, $z_{\min}$, $\tau_{\max,i}$, $\forall i \in \{1,\dots,K\}$
for $(\ell, j) \in \{K,\dots,2,1\} \times \{K,\dots,2,1\}$
  $\mathcal{I}_{\max} \leftarrow 0, \text{temp} \leftarrow 0$
  if $j \leq \ell$
    $U_1 \leftarrow \{1,\dots,j\}$, $U_2 \leftarrow \{j+1,\dots,\ell\}$, then **compute** λ from (35)
    if (36) is satisfied
      $z_i \leftarrow z_{\min}\, \forall i > j$, $\tau_i \leftarrow \tau_{\max,i}\, \forall i \in \bar{U}_2$
      Find $\tau_i\, \forall i \in U_1$ s.t. (37)
    end if
  else
    $U_1 \leftarrow \{1,\dots,\ell\}$, $U_3 \leftarrow \{\ell+1,\dots,j\}$, then **compute** λ from (39)
    if (40) is satisfied
      $z_i \leftarrow z_{\min}\, \forall i \in U_4, \tau_i \leftarrow \tau_{\max,i}\, \forall i > \ell, \tau_i \leftarrow \frac{z_{\min}}{4\lambda^2}\, \forall i \in U_3$
      Find $\tau_i\, \forall i \in U_1$ s.t. (41)
    end if
  end if
  $z_i \leftarrow 4\lambda^2 \tau_i \quad \forall i \in U_1, \text{temp} \leftarrow \sum_{i=1}^{K} \sqrt{z_i \tau_i}$
  if $(\text{temp} > \mathcal{I}_{\max})$
    $\mathcal{I}_{\max} \leftarrow \text{temp}, \boldsymbol{\tau}^* \leftarrow \boldsymbol{\tau}, \boldsymbol{z}^* \leftarrow \boldsymbol{z}$
  end if
  Solve (29) **and** (30) **for** $\nu_i\, \forall i$ **and** $o_i\, \forall i$
  if $o_i \geq 0, \nu_i \geq 0 \quad \forall i$
    Terminate.
  end if
end for
Output: $\boldsymbol{z}^*, \boldsymbol{\tau}^*$

variables are calculated in addition to evaluating the objective function to keep track of the best feasible solution found in different configurations. Finally, the dual variables are calculated to assess optimality of the obtained solution and terminate the algorithm accordingly.

B. Photometric flickering

The considered optimization frameworks allow temporal fluctuations of the LED excitation current, which might result in photometric flickering that can be hazardous for human health and productivity, when it exceeds certain levels. Similar to the flicker percent metric proposed in [30], we define the flickering metric in the presented resource allocation context as

$$F_{\%} = \frac{I_{\max} - I_{\min}}{I_{\max} + I_{\min}} \times 100\%, \tag{42}$$

where $I_{\max} = \max_{\boldsymbol{h}\in\mathcal{H}} I\left(\boldsymbol{z}_p(\boldsymbol{h}), \boldsymbol{\tau}_p(\boldsymbol{h})\right)$ and $I_{\min} = \min_{\boldsymbol{h}\in\mathcal{H}} I\left(\boldsymbol{z}_p(\boldsymbol{h}), \boldsymbol{\tau}_p(\boldsymbol{h})\right)$, such that $\mathcal{H}$ represents the set of feasible realizations, $\boldsymbol{z}_p(\boldsymbol{h})$, and $\boldsymbol{\tau}_p(\boldsymbol{h})$ are the Pareto optimized allocation vectors (solution of $(\tilde{\mathbf{P}}\mathbf{3})$) when channel realization vector $\boldsymbol{h}$ is assumed.

V. Spectral efficiency-Illumination Tradeoff

In this section, we investigate the MOOP between the SE and the illumination to obtain the Pareto-frontier curve. The MOOP enables us to tune the priority level of the objective functions. Moreover, it shows the loss of SE/illumination when illumination/SE is maximized. To this end, we adopt the scalarization approach to solve the MOOP , where a weighted sum of the normalized objective functions is maximized according to

$$\begin{aligned} (\mathbf{P3}) \quad \max_{\mathbf{z},\boldsymbol{\tau}} \quad & \frac{\alpha}{\eta_{\mathrm{SE}}^{\max}} \sum_{i=1}^{K} \frac{\tau_i}{2} \ln\left(1 + \frac{\gamma_i z_i}{\tau_i}\right) + \frac{1-\alpha}{\mathcal{I}_{\max}} \sum_{i=1}^{K} \sqrt{z_i \tau_i} \\ \text{subject to} \quad & \mathrm{C1} - \mathrm{C5}, \end{aligned}$$

where $\eta_{\mathrm{SE}}^{\max}$ and $\mathcal{I}_{\max}$ are the optimal objective values of $(\tilde{\mathbf{P}}\mathbf{1})$ and $(\tilde{\mathbf{P}}\mathbf{2})$ respectively. $(\mathbf{P3})$ is clearly convex, as the constraints represent a convex set which was discussed before, and it is a maximization problem with positive weighted sum of concave functions. We express the Lagrangian of this problem as follows:

$$\begin{aligned} \mathcal{L} = {} & \frac{\alpha}{\eta_{\mathrm{SE}}^{\max}} \sum\nolimits_{i=1}^{K} \frac{\tau_i}{2} \ln\left(1 + \frac{\gamma_i z_i}{\tau_i}\right) + \frac{1-\alpha}{\mathcal{I}_{\max}} \sum\nolimits_{i=1}^{K} \sqrt{z_i \tau_i} + \mu \left(P_{\mathrm{M}} - \sum\nolimits_{i=1}^{K} z_i\right) \\ & + \sum\nolimits_{i=1}^{K} o_i \left(z_i - z_{\min}\right) + \sum\nolimits_{i=1}^{K} \nu_i \left(\tau_{i,\max} - \tau_i\right) + \lambda \left(1 - \sum\nolimits_{i=1}^{K} \tau_i\right) + \sum\nolimits_{i=1}^{K} \kappa_i \left(\tau_i - \tau_{\min}\right). \end{aligned}$$

The KKT stationarity conditions of $(\mathbf{P3})$ are:

$$\frac{\partial \mathcal{L}}{\partial z_i} = \frac{\alpha}{2\eta_{\mathrm{SE}}^{\max}} \frac{\gamma_i}{1 + \gamma_i z_i/\tau_i} + \frac{1-\alpha}{2\mathcal{I}_{\max}} \sqrt{\frac{\tau_i}{z_i}} - \mu + o_i = 0 \quad \forall i, \tag{43}$$

$$\frac{\partial \mathcal{L}}{\partial \tau_i} = \frac{\alpha}{2\eta_{\mathrm{SE}}^{\max}} \left(\ln\left(1 + \frac{\gamma_i z_i}{\tau_i}\right) - \frac{\gamma_i z_i}{\tau_i + \gamma_i z_i}\right) + \frac{1-\alpha}{2\mathcal{I}_{\max}} \sqrt{\frac{z_i}{\tau_i}} - \nu_i - \lambda + \kappa_i = 0 \quad \forall i, \tag{44}$$

in addition to $\mathrm{C1}-\mathrm{C5}$, (8) and (9). Due to the inherent complexity in solving (43) and (44) for z_i/τ_i in terms of the Lagrange multipliers, we use the bound $\ln(1+x) \leq \sqrt{x}$ to upper bound the objective function of $\mathbf{(P3)}$. We formulate $\mathbf{(\tilde{P}3)}$ using that upper bound as a surrogate objective function. Thus, the optimal solution of $\mathbf{(\tilde{P}3)}$ is sub-optimal for $\mathbf{(P3)}$. However, due to similarity in behavior of the bound and the original objective function, we shall see in the simulation results in section VII that the Pareto-frontiers obtained by optimizing the bound and the original objective function are close. The resulting surrogate optimization problem can be expressed as:

$$\begin{aligned} \mathbf{(\tilde{P}3)} \quad \max_{\mathbf{z},\boldsymbol{\tau}} \quad & \frac{\alpha}{\eta_{\mathrm{SE}}^{\max}} \sum_{i=1}^{K} \frac{1}{2} \sqrt{\gamma_i \tau_i z_i} + \frac{1-\alpha}{\mathcal{I}_{\max}} \sum_{i=1}^{K} \sqrt{z_i \tau_i} \\ \text{subject to} \quad & \mathrm{C1}-\mathrm{C5}. \end{aligned}$$

We express the Lagrangian of $\mathbf{(\tilde{P}3)}$ as:

$$\begin{aligned} \mathcal{L}_{\mathrm{ub}} = & \sum\nolimits_{i=1}^{K} \Gamma_i \sqrt{z_i \tau_i} + \mu \left(P_{\mathrm{M}} - \sum\nolimits_{i=1}^{K} z_i \right) + \sum\nolimits_{i=1}^{K} o_i \left(z_i - z_{\min} \right) + \sum\nolimits_{i=1}^{K} \nu_i \left(\tau_{i,\max} - \tau_i \right) \\ & + \lambda \left(1 - \sum\nolimits_{i=1}^{K} \tau_i \right) + \sum\nolimits_{i=1}^{K} \kappa_i \left(\tau_i - \tau_{\min} \right), \end{aligned} \tag{45}$$

where $\Gamma_i = \frac{\alpha}{2\eta_{\mathrm{SE}}^{\max}} \sqrt{\gamma_i} + \frac{1-\alpha}{\mathcal{I}_{\max}}$.
The KKT conditions of $\mathbf{(\tilde{P}3)}$ are:

$$\frac{\partial \mathcal{L}_{\mathrm{ub}}}{\partial z_i} = 0 \implies \frac{z_i^*}{\tau_i^*} = \frac{\Gamma_i^2}{4\left(\mu - o_i\right)^2} \quad \forall i, \tag{46}$$

$$\frac{\partial \mathcal{L}_{\mathrm{ub}}}{\partial \tau_i} = 0 \implies \frac{\tau_i^*}{z_i^*} = \frac{\Gamma_i^2}{4\left(\nu_i + \lambda - \kappa_i\right)^2} \quad \forall i, \tag{47}$$

in addition to $\mathrm{C1}-\mathrm{C5}$, (9) and (8).

As mentioned in the two former sections, we avoid the exponential complexity of searching over all possible combinations of the inequalities Lagrange multipliers by restricting our search space to solutions having special structures. For this problem we look for solutions of two possible forms:

(i) $\mathbf{z^*} = \left[z_1^*, \ldots, z_j^*, z_{\min}, \ldots, z_{\min} \right], \boldsymbol{\tau^*} = \left[\tau_{\max,1}, \ldots, \tau_{\max,f-1}, \tau_f^*, \ldots, \tau_l^*, \tau_{\min}, \ldots, \tau_{\min} \right]$.

(ii) $\mathbf{z^*} = \left[z_1^*, \ldots, z_j^*, z_{\min}, \ldots, z_{\min} \right], \boldsymbol{\tau^*} = \left[\tau_{\max,1}, \ldots, \tau_{\max,f-1}, \tau_f^*, \ldots, \tau_l^*, \tau_{\max,l+1}, \ldots, \tau_{\max,K} \right]$.

We choose the previous structures to limit the complexity of solving the KKT system to $O\left(K^3\right)$. The structure (i) is chosen inspired by the SE maximization problem solution, while the structure (ii) is chosen inspired by the superposition of the structures of both the SE and the illumination maximization problems. In contrast to SE maximization problem, one user at most can fall into Case 1 in Table III otherwise the KKT system will have no solution. However, similar to the SE problem, we have three possible solution structures: (i) $N_\tau > 1, j = f$, (ii) $N_\tau > 1, j < f$,

TABLE III: Inequality constraints multipliers configurations for $(\tilde{\mathbf{P3}})$. The optimal (τ_i, z_i) pair is indicated below each case.

		$o_i = 0$		$o_i \neq 0$	
$\nu_i = 0$	$\kappa_i = 0$	**Case 1** (τ_i^*, z_i^*)	$\frac{z_i^*}{\tau_i^*} = \frac{\Gamma_i^2}{4\mu^2}$, $\frac{\tau_i^*}{z_i^*} = \frac{\Gamma_i^2}{4\lambda^2}$	**Case 4** $(\tau_i^*, z_{\min})$	$\frac{z_{\min}}{\tau_i^*} = \frac{\Gamma_i^2}{4(\mu - o_i)^2}$, $\frac{\tau_i^*}{z_{\min}} = \frac{\Gamma_i^2}{4\lambda^2}$
	$\kappa_i \neq 0$	**Case 3** $(\tau_{\min}, z_i^*)$	$\frac{z_i^*}{\tau_{\min}} = \frac{\Gamma_i^2}{4\mu^2}$, $\frac{\tau_{\min}}{z_i^*} = \frac{\Gamma_i^2}{4(\lambda - \kappa_i)^2}$	**Case 5** $(\tau_{\min}, z_{\min})$	$\frac{z_{\min}}{\tau_{\min}} = \frac{\Gamma_i^2}{4(\mu - o_i)^2}$, $\frac{\tau_{\min}}{z_{\min}} = \frac{\Gamma_i^2}{4(\lambda - \kappa_i)^2}$
$\nu_i \neq 0$	$\kappa_i = 0$	**Case 2** $(\tau_{\max,i}, z_i^*)$	$\frac{z_i^*}{\tau_{\max,i}} = \frac{\Gamma_i^2}{4\mu^2}$, $\frac{\tau_{\max,i}}{z_i^*} = \frac{\Gamma_i^2}{4(\nu_i + \lambda)^2}$	**Case 6** $(\tau_{\max,i}, z_{\min})$	$\frac{z_{\min}}{\tau_{\max,i}} = \frac{\Gamma_i^2}{4(\mu - o_i)^2}$, $\frac{\tau_{\max,i}}{z_{\min}} = \frac{\Gamma_i^2}{4(\nu_i + \lambda)^2}$

and (iii) $N_\tau = 1$.

(i) For $N_\tau > 1, j = f$, we calculate λ as

$$\lambda = \frac{\frac{1}{2}\sqrt{\left(P_{\mathrm{M}} - \left(K - j - \frac{\sum_{i\in U_4}\Gamma_i^2}{\Gamma_j^2}\right) z_{\min}\right)}}{\sqrt{\left(\frac{1 - \sum_{i=1}^{f-1}\tau_{\max,i} - (K-\ell)\tau_{\min} S + \bar{S}\sum_{i=l+1}^{K}\tau_{\max,i}}{\Gamma_j^2} + \frac{\sum_{i\in U_2}\tau_{\max,i}\Gamma_i^2}{\Gamma_j^4}\right)}}, \tag{48}$$

where S is a binary variable that is set to either 1 or 0 to represent the first or the second solution structure, respectively, and $\bar{S} = 1 - S$. Then μ is calculated from: $\mu = \dfrac{\Gamma_j^2}{4\lambda}$. (49)

Finally all primal variables can be obtained as follows:

$$z_i^* = \frac{\tau_{\max,i}\Gamma_i^2}{4\mu^2}\ \forall i \in U_2,\ U_2 \triangleq \{1, .., j-1\}, \tag{50}$$

$$z_j^* = P_{\mathrm{M}} - z_{\min}(K - j) - \sum\nolimits_{i\in U_2} z_i^*, \tag{52}$$

$$\tau_i^* = \frac{z_{\min}\Gamma_i^2}{4\lambda^2}\ \forall i \in U_4,\ U_4 \triangleq \{j+1, .., l\}, \tag{51}$$

$$\tau_j^* = \bar{\tau} - \sum\nolimits_{i\in U_4}\tau_{\max,i}, \tag{53}$$

where $\bar{\tau} = 1 - \tau_{\min}(K - f) S + \bar{S}\sum_{i=l+1}^{K}\tau_{\max,i}$.

(ii) For $N_\tau > 1, j < f$, we get λ from,

$$\lambda = \frac{1}{2}\sqrt{\frac{z_{\min}\sum_{i\in U_4}\Gamma_i^2}{1 - \tau_{\min}(K - \ell) S + (1 - S)\sum_{i=l+1}^{K}\tau_{\max,i} - \sum_{i\in U_2}\tau_{\max,i}}} \tag{54}$$

where $U_2 \triangleq \{1, \ldots, j\}$, and $U_4 \triangleq \{j+1, \ldots, l\}$, and we calculate μ from,

$$\mu = \frac{1}{2}\sqrt{\frac{\sum_{i\in U_2}\Gamma_i^2}{P_{\mathrm{M}} - z_{\min}(K - j)}}, \tag{55}$$

then $z_i^* \quad \forall i \in U_2, \tau_i^* \quad \forall i \in U_4$ are calculated from (50), (51) respectively.

(iii) For $N_\tau = 1$, μ is calculated from $\mu = \dfrac{1}{2}\sqrt{\sum_{i=1}^{j}\Gamma_i^2 / (P_{\mathrm{M}} - z_{\min}(K - j))}$. (56)

Then $\tau_f^* = 1 - \sum_{i=1}^{f-1}\tau_{\max,i} - \tau_{\min}(K - l) S + (1 - S)\sum_{i=l+1}^{K}\tau_{\max,i}$, and $z_i^* = \frac{\Gamma_i^2\tau_i^*}{4\mu^2} \quad \forall i \leq j$.

TABLE IV: Default Simulation Parameters.

$N_0 = 10^{-21}$ W/Hz	$B_{\rm v} = 20$ MHz	$R_{\rm PD} = 0.6$ A/W	$P_{\rm cr} = 200$ mW	$L_{\max}$= 3000 lux	$n = 1.76$
$\tau_{\min} = 1 \times 10^{-2}$	$K = 30$	$R_{\rm th} = 2.5 \times 10^6$bps	$P_M = 1000$ W	$R_{\rm outer} = 25$ m	$\phi_{\rm A} = 50^\circ$
$\psi_{\rm A} = \tan^{-1}\left(\frac{25}{6.75}\right)$	H=6.75 m	$I_o = 1 \times 10^{-12}$A	$A_{\rm PD} = 4\,{\rm cm}^2$	$\eta_\phi = 7000$ lm/A	

In Algorithm I with ($\mathcal{A} = 0$), we first assume that the first solution structure is optimal, search through different inequalities multipliers configurations (i)–(iii) in a very similar way to Algorithm I. Then for each configuration, we calculate the primal variables as per the previous discussion. We keep track the of best found feasible configuration and calculate the dual variables and terminate in case optimality is reached (all KKT conditions are satisfied). In case the algorithm didn't terminate after scanning all possibilities for the first solution structure, we repeat the same steps whilst considering the second solution structure.

VI. Simulation results

The simulation setup consists of a VLC transmitter similar to the scenario shown in Fig. 1 with a 6.75 m clearance from the receivers plane. The transmitter coverage is represented by a circle with radius $R_{\rm outer} = H\tan(\psi_{\rm A})$. We assume that users are distributed over a circular disc with inner and outer radii $R_{\rm inner}$ and $R_{\rm outer}$, respectively. All the users' receivers are assumed to have horizontal orientation as the transmitter. The average SE and illumination results are calculated based on 1000 realizations of users placed at random locations according to a uniform distribution. Unless otherwise stated, we use the simulation parameters listed in Table IV. In the conducted simulations, infeasible realizations have zero contribution to the average SE and illumination performance metrics.

A. SE and Illumination Optimization Simulations

In this section, we study the average optimized SE performance of the considered VLC system for different proposed algorithms, i.e., I, II, III. Moreover, we study the average optimized illumination performance of algorithm IV. As a benchmark, we use the interior point method algorithm that gives optimal solution for the considered problem due to its convexity. In the first simulation example, we study the effect of changing the service area of the proposed system on the SE performance. To this end, we vary $R_{\rm inner}$ and keep $R_{\rm outer}$ constant for different values of

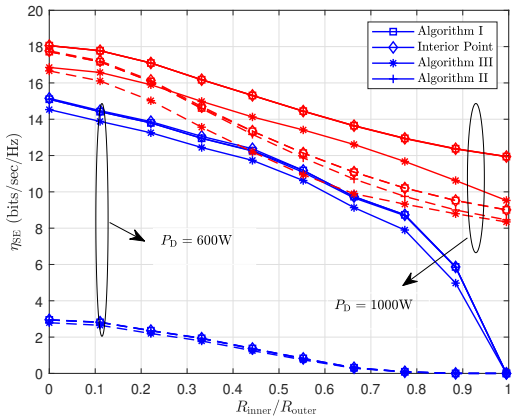

Fig. 2: Average SE vs $R_{\rm inner}/R_{\rm outer}$, $P_{\rm M} = \{600, 1000\}$ Watt, $K = 20$

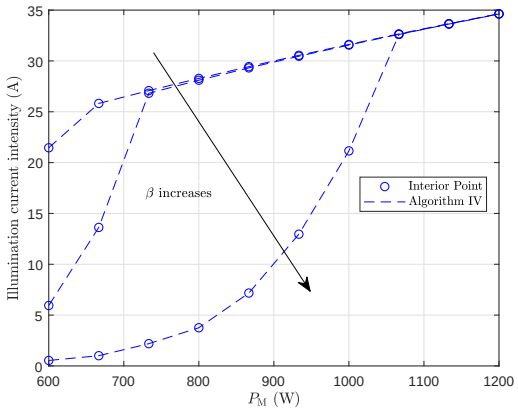

Fig. 3: Average Illum. current intensity vs. $P_{\rm M}$, $\beta = \{0.005, 0.188, 0.19\}$

$P_{\rm M}$ as shown in Fig. 2. It can be noticed that as $R_{\rm inner}$ increases, the SE performance degrades because the users get far from the transmitter, which worsens the channels gain.

As for the relative performance of our proposed algorithms and the interior point solution, we observe that Algorithm I proves its efficiency and achieves similar performance to the interior point method for different ranges of $P_{\rm M}$ and $R_{\rm inner}$. As for Algorithm II, it has a negligible gap with Algorithm I for small and large values of $P_{\rm M}$ as can be seen in the solid curves of Fig. 2, while it has a small gap for the mid-range of $P_{\rm M}$ as can be noticed for scenario 2 results shown in the dashed curves of Fig. 2, where $R_{\rm outer} = 30$ m, $\phi_{\rm a} = 40°$, $\tau_{\rm min} = 1.5 \times 10^{-3}$ sec., $R_{\rm th} = 3.45 \times 10^5$ bps, and $\psi_{\rm A} = \tan^{-1}\left(\frac{30}{6.75}\right)$. The superiority of Algorithm I over Algorithm II attributes to its better time allocation performance, this appears in scenarios where feasibility space gets tight for power allocation variables while it is not the case for time allocation variables. On the other hand, the performance gap between Algorithm I and algorithm III increases with $P_{\rm M}$ as shown in Fig. 2, which is due to the uniform power allocation of algorithm III.

In the second simulation example, we study the performance of the proposed illumination optimization algorithm (Algorithm IV) and the optimal performance (using interior point method) versus different system parameters. We study the illumination performance versus $P_{\rm M}$ for different β in Fig. 3. As $P_{\rm M}$ increases, the feasibility region gets larger, thus, the average illumination increases as shown in Fig. 3. The presented result shows also that as β increases, the illumination gains of increasing $P_{\rm M}$ become more significant. It is worthy emphasizing that Algorithm IV performance matches the interior point method performance as shown in Fig. 3.

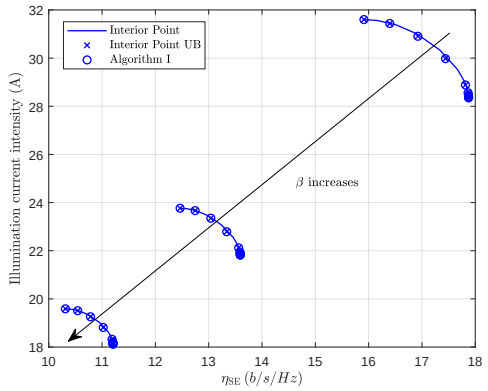

Fig. 4: Average SE-Illumination Pareto front for $\beta = \{0.1, 0.192, 0.193\}$, $R_{\mathrm{th}} = 2.55 \times 10^6$ bps

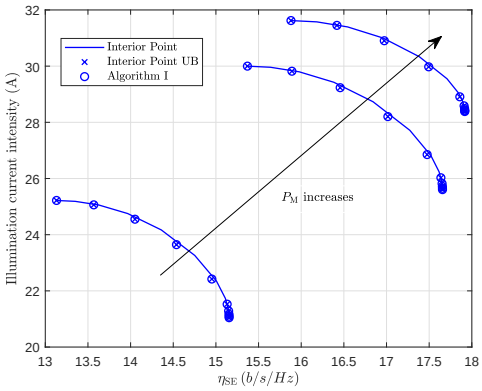

Fig. 5: Average SE-Illumination Pareto front for $\beta = 0.005$,$R_{\mathrm{th}} = 2.55 \times 10^6$,$P_{\mathrm{M}} = \{850, 900, 1000\}$W

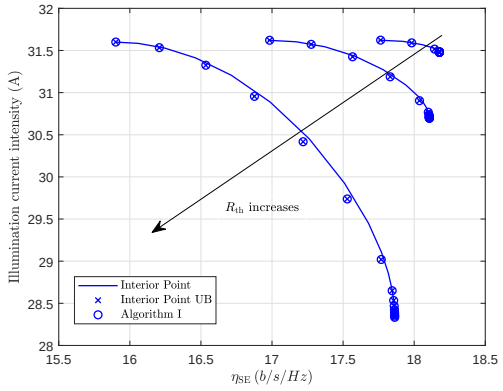

Fig. 6: Average SE-Illumination Pareto front for $R_{\mathrm{th}} = \{2.45, 2.5, 2.55\} \times 10^6$ bps, $\beta = 0.005$

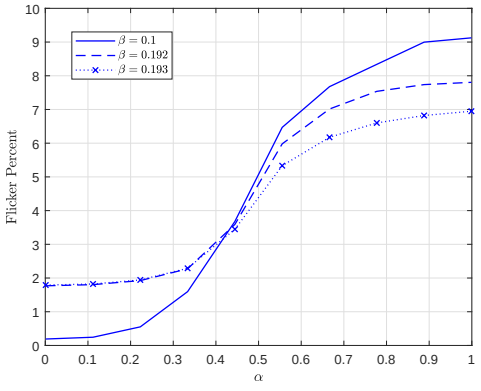

Fig. 7: Flicker Percentage vs α for $\beta = \{0.1, 0.192, 0.193\}$, $R_{\mathrm{th}} = 2.55 \times 10^6$ bps

B. SE–Illumination optimization simulations

In this section, we study the tradeoff relationship between the SE and the illumination using Algorithm I and compare it with the interior point algorithm solution of the original problem ($\mathbf{P3}$) and the upper bounded problem ($\tilde{\mathbf{P}}\mathbf{3}$). We uniformly sample the optimization weight α, and average obtained performance vectors for each α value. Moreover, we monitor the flicker percentage metric for the interior point method solution of Pareto-optimal solution ($\mathbf{P3}$). The first set of SE-illumination Pareto fronts shows the tradeoff relationship for different β in Fig.

4. As β increases, illumination intensity and SE performance degrades, because increasing β results in a tighter feasibility region and higher chances for infeasibile realizations.

Next, the average SE-illumination Pareto front obtained by the three aforementioned methods are plotted for different values of P_{M} in Fig. 5. The simulation results show that as P_{M} increases, the achievable average SE-illumination trade-off is improved as the increased power budget makes higher SE and illumination intensities attainable. Then, the Pareto front is studied with the change of R_{th} for $\beta = 0.005$ as shown in Fig. 6 . As R_{th} increases, the Pareto front curve is degraded at the SE side without changing the maximum illumination. Changing R_{th} does not affect the illumination performance function if the energy harvesting requirement is tolerant enough. All the considered simulations have shown that Algorithm I performance matches the performance of optimal solution to the surrogate optimization problem $(\tilde{\mathbf{P3}})$ and it is so close to the optimal solution of the original problem $(\mathbf{P3})$.

In addition, we present the temporal behavior of the MOOP-based allocation in Fig. 7 as α changes for different energy harvesting requirements. It can be seen that for small α values (when emphasis is put on illumination maximization) the experienced flicker is much less than that for large values of α. This can be attributed to the heavy dependency of the SE maximization solution on the channel coefficients of different users, whereas illumination maximization solution is affected by the channel coefficients only through the energy harvesting constraint. Consequently it can be seen that for large β values flicker increases when illumination is maximized as the solution dependency on channel gains is increased. On the other hand, the SE maximization gets less sensitive to channel gains variations the space of allocation choices itself diminishes and the scheduler is forced to allocate more resources to users suffering small channel gains. Furthermore, it can be noticed that the maximum flicker percentage seen is highly tied to the average illumination performance gap between the solutions of SE and illumination maximization.

Studying the tradeoff strength is essential in providing good guidelines for system designers. One way is to investigate the skewness of the Pareto front (the ratio of SE loss to illumination loss) change with different parameters (R_{th}, β, and P_{M}). It is observed that as the constraints get looser (β or R_{th} decreases or P_{M} increases) the SE losses due to illumination optimization becomes more significant than the illumination losses due to optimizing SE. For this purpose, we study the the SE loss percentage defined as the difference between maximum achievable SE and the highest attainable SE when illumination is maximized, divided by maximum SE. In addition to that, we study the illumination loss that has a similar definition to the SE loss. In

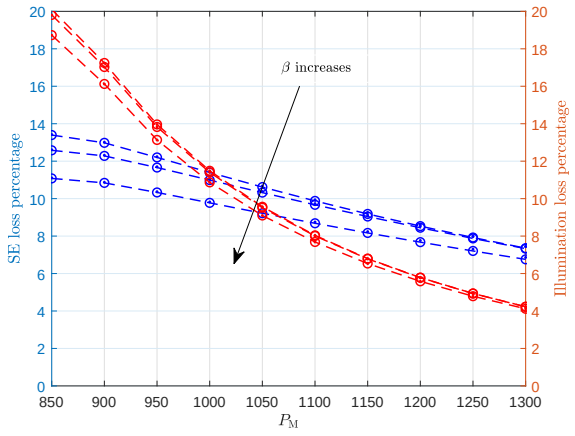

Fig. 8: SE loss percentage vs. P_{M} for $\beta = \{0.005, 0.1, 0.15\}$, $R_{\mathrm{th}} = 2.55 \times 10^6$ bps

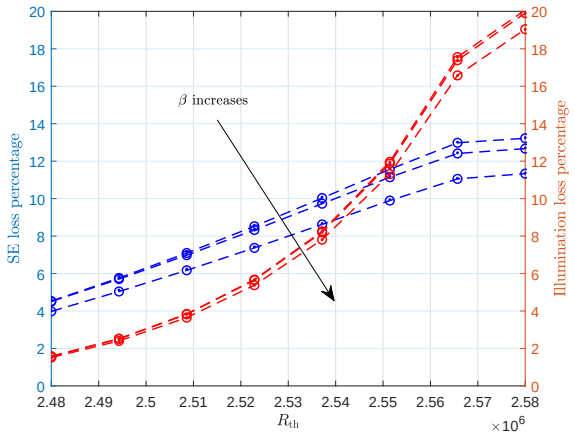

Fig. 9: Illumination loss percentage vs R_{th} for $\beta = \{0.005, 0.1, 0.15\}$

Fig. 8, we observe that as P_{M} increases, both the SE and illumination loss percentages exhibit different trend either a decreasing, unimodal, or increasing depending on the value of β. It is beneficial to monitor when the loss becomes significant to consider it in the design process. Fig. 9 shows the SE and illumination loss versus the R_{th} for different β. It is worthy to note that the loss is significant in both SE and illumination for negligible harvesting and high minimum rate requirements. However, loss decreases with the increase of β and become significant for the illumination at high R_{th}.

VII. CONCLUSION

MOOP is a powerful optimization framework to deal with resource allocation problems for dynamic TDMA outdoor VLC systems, where maximizing the overall system SE and illumination capabilities become of crucial importance. To characterize the Pareto front of the SE-illumination region, we solved the marginal optimization problems, maximizing the SE and maximizing the illumination. Then, inspired by the proposed solution, we suggested an algorithm that obtain the Pareto front of the SE-illumination region. Numerical results showed a close match between our algorithms and the optimal solution. Moreover, it was shown that the more the weight given to SE maximization the more photometric flickering increases. It was shown that flickering is affected by other system parameters as energy harvesting requirement, minimum allocated time, and minimum rate requirement, in addition to channel statistics. As a future work, a control mechanism can be developed to maintain flickering within permissible level for eye-safety and

productivity. Furthermore, it was found that the tradeoff between the illumination service and the Communications service severity increases as the available power budget is reduced, or the individual rate constraints become strict. Possible follow up future studies, include but are not limited to, interference-based scenarios, MIMO setups, and hybrid VLC/RF configurations.

APPENDIX A
ENERGY HARVESTING LOWER BOUND

$$\textbf{(P0)} \quad \min_{\mathbf{z},\boldsymbol{\tau}} \quad \sum_{j=1}^{K} \sqrt{\tau_j z_j} \ln\left(1+\frac{h_i}{I_o}\sqrt{\frac{z_j}{\tau_j}}\right)$$
$$\text{subject to} \quad \mathrm{C1}: \sum_{i=1}^{K} z_i = P_{\mathrm{M}}, \ \ \mathrm{C2}: \sum_{i=1}^{K} \tau_i = 1, \ \mathrm{C3}: \tau_i \geq \tau_{\min} \, \forall i, \ \ \mathrm{C4}: z_i \geq z_{\min} \, \forall i,$$

The Lagrangian formulation of $\textbf{(P0)}$ is given by:

$$\mathcal{L}_{\mathrm{H}} = \sum_{i=1}^{K} \sqrt{\tau_i z_i} \ln\left(1+\frac{h_i}{I_o}\sqrt{\frac{z_j}{\tau_j}}\right) + \mu\left(P_{\mathrm{M}} - \sum_{i=1}^{K} z_i\right) + \lambda\left(1 - \sum_{i=1}^{K} \tau_i\right)$$
$$+ \sum_{i=1}^{K} o_i \left(z_{\min} - z_i\right) + \sum_{i=1}^{K} \kappa_i \left(\tau_{\min} - \tau_i\right). \tag{57}$$

The KKT conditions for $\textbf{(P0)}$ can be summarized as follows

$$\frac{\partial \mathcal{L}_{\mathrm{H}}}{\partial z_i} = g_{j,1}\left(\sqrt{\frac{z_i}{\tau_i}}\right) - \mu - o_i = 0, \ g_{j,1}(x) = \left(\frac{h_j}{I_o\left(2\left(1+\frac{h_j x}{I_o}\right)\right)} + \frac{\ln\left(1+\frac{h_j x}{I_o}\right)}{2x}\right),$$

$$\frac{\partial \mathcal{L}_{\mathrm{H}}}{\partial \tau_i} = g_{j,2}\left(\sqrt{\frac{z_i}{\tau_i}}\right) - \lambda - \kappa_i = 0, \ g_{j,2}\left(x\right) = 0.5\left(x\ln\left(1+\frac{h_j x}{I_o}\right) - \frac{h_j x^2}{\left(I_o\left(1+\frac{h_j x}{I_o}\right)\right)}\right),$$

$$o_i \left(z_i - z_{\min}\right) = 0 \ \ \forall i, \ \kappa_i \left(\tau_i - \tau_{\min}\right) = 0 \ \ \forall i, \ o_i \geq 0, \ \ \kappa_i \geq 0, \ \ \forall i, \mathrm{C1}, \mathrm{C2}, \mathrm{C3}, \mathrm{C4}.$$

The necessity of KKT conditions optimality is imposed in this problem by the linearity of the constraints. It can be noticed that for case 2, case 3, and case 4, the primal variables and inequalities multipliers are the same for all users having the same configuration, such that: $o_i = o_m$ and $\kappa_i = \kappa_m \ \forall i \in U_m$. Moreover, it can be deduced that $z_i^* = z_{U_2} \forall i \in U_2$ and

TABLE V: Inequality constraints multipliers configurations for $\mathbf{(P0)}$. The optimal (τ_i, z_i) pair is indicated below each case.

	$o_i = 0$		$o_i \geq 0$	
$\kappa_i = 0$	**Case 1** (τ_i^*, z_i^*)	$\sqrt{\frac{z_i^*}{\tau_i^*}} = g_{j,1}^{-1}(\mu) = g_{j,2}^{-1}(\lambda)$	**Case 3** $(\tau_i^*, z_{\min})$	$\sqrt{\frac{z_{\min}}{\tau_i^*}} = g_{j,1}^{-1}(\mu + o_i) = g_{j,2}^{-1}(\lambda)$
$\kappa_i \geq 0$	**Case 2** $(\tau_{\min}, z_i^*)$	$\sqrt{\frac{z_i^*}{\tau_{\min}}} = g_{j,1}^{-1}(\mu) = g_{j,2}^{-1}(\lambda + \kappa_i)$	**Case 4** $(\tau_{\min}, z_{\min})$	$\sqrt{\frac{z_{\min}}{\tau_{\min}}} = g_{j,1}^{-1}(\mu + o_i) = g_{j,2}^{-1}(\lambda + \kappa_i)$

$\tau_i^* = \tau_{U_3}\ \forall i \in U_3$. By plugging the previous relations (stationarity conditions) shown in Table V in C1 and C2, we get

$$\sum_{i \in U_1} \tau_i^* + (n_2 + n_4)\,\tau_{\min} + n_3 \frac{z_{\min}}{\left(g_{j,2}^{-1}(\lambda)\right)^2} = 1, \tag{58}$$

$$\left(g_{j,1}^{-1}(\mu)\right)^2 \sum_{i \in U_1} \tau_i^* + n_2 \left(g_{j,1}^{-1}(\mu)\right)^2 \tau_{\min} + (n_3 + n_4)\, z_{\min} = P_{\mathrm{M}}, \tag{59}$$

where n_m represents the cardinality of the set U_m. It can be seen clearly that what only matters in the solution structure is the cardinalities of U_1, U_2, U_3, and U_4 due to the problem symmetry with respect to the optimization parameters.

- If $n_1 > 0$ i.e. $g_{j,1}^{-1}(\mu) = g_{j,2}^{-1}(\lambda)$, and by checking the monotonicity of $g_{j,1}(.)$, $g_{j,2}(.)$, and consequently their inverses $g_{j,1}^{-1}(.)$, and $g_{j,2}^{-1}(.)$, respectively as follows

$$g'_{j,1}(x) = \underbrace{\frac{1}{2x^2}\left(\frac{\frac{h_j x}{I_o}}{\frac{h_j x}{I_o}+1} - \ln\left(\frac{h_j x}{I_o}+1\right)\right)}_{\leq 0} + \underbrace{\frac{d}{dx}\frac{h_j}{I_o\left(2\left(1+\frac{h_j x}{I_o}\right)\right)}}_{\leq 0},$$

$$g'_{j,2}(x) = \frac{1}{2}\left(\frac{\left(\frac{h_j x}{I_o}\right)^2}{\left(\frac{h_j x}{I_o}+1\right)^2} \underbrace{- \frac{\frac{h_j x}{I_o}}{\frac{h_j x}{I_o}+1} + \ln\left(\frac{h_j x}{I_o}+1\right)}_{\geq 0}\right).$$

It can be deduced that there is a one-to-one correspondence between μ and λ. Thus, equations (58),(59) reduce to:

$$\sum_{i \in U_1} \tau_i^* = 1 - (n_2 + n_4)\,\tau_{\min} - n_3 z_{\min} \frac{1 - n_4 \tau_{\min}}{P_{\mathrm{M}} - n_4 z_{\min}}, \tag{60}$$

$$g_{j,1}^{-1}(\mu) = \sqrt{\frac{P_{\mathrm{M}} - n_4 z_{\min}}{1 - n_4 \tau_{\min}}}. \tag{61}$$

Consequently, it can be found that $\kappa_{U_2}=0, o_{U_3}=0$,

$$\mu = g_{j,1}\left(\sqrt{\frac{P_{\mathrm{M}}-n_4 z_{\min}}{1-n_4\tau_{\min}}}\right), \quad (62)$$

$$\lambda = g_{j,2}\left(\sqrt{\frac{P_{\mathrm{M}}-n_4 z_{\min}}{1-n_4\tau_{\min}}}\right), \quad (63)$$

$$z_{U_2} = \tau_{\min}\frac{P_{\mathrm{M}}-n_4 z_{\min}}{1-n_4\tau_{\min}}, \quad (64)$$

$$\tau_{U_3} = z_{\min}\frac{1-n_4\tau_{\min}}{P_{\mathrm{M}}-n_4 z_{\min}}, \quad (65)$$

$$o_{U_4} = g_{j,1}\left(\sqrt{\frac{z_{\min}}{\tau_{\min}}}\right)-\mu, \quad (66)$$

$$\kappa_{U_4} = g_{j,2}\left(\sqrt{\frac{z_{\min}}{\tau_{\min}}}\right)-\lambda, \quad (67)$$

$\tau_i^*\ \forall i\in U_1$ can be set to any values satisfying (60) and C3, with $z_i^*=\tau_i^*\frac{P_{\mathrm{M}}-n_4 z_{\min}}{1-n_4\tau_{\min}}\ \forall i\in U_1$.

- If $n_1=0$, equations (58),(59) reduce to

$$\lambda = g_{j,2}\left(\sqrt{\frac{n_3 z_{\min}}{1-(n_2+n_4)\tau_{\min}}}\right), \quad (68)$$

$$\mu = g_{j,1}\left(\sqrt{\frac{P_{\mathrm{M}}-(n_3+n_4)z_{\min}}{n_2\tau_{\min}}}\right). \quad (69)$$

Therefore,

$$z_{U_2} = \frac{P_{\mathrm{M}}-(n_3+n_4)z_{\min}}{n_2}, \quad (70)$$

$$\tau_{U_3} = \frac{1-(n_2+n_4)}{n_3}, \quad (71)$$

$$o_{U_4} = g_{j,1}\left(\sqrt{\frac{z_{\min}}{\tau_{\min}}}\right)-\mu, \quad (72)$$

$$\kappa_{U_2} = g_{j,2}\left(\sqrt{\frac{P_{\mathrm{M}}-(n_3+n_4)z_{\min}}{n_2\tau_{\min}}}\right)-\lambda, \quad (73)$$

$$o_{U_3} = g_{j,1}\left(\sqrt{\frac{n_3 z_{\min}}{1-(n_2+n_4)\tau_{\min}}}\right)-\mu, \quad (74)$$

$$\kappa_{U_4} = g_{j,2}\left(\sqrt{\frac{z_{\min}}{\tau_{\min}}}\right)-\lambda. \quad (75)$$

The optimal solution of $(\mathbf{P0})$ can be obtained by searching the feasibility space of n_1, n_2, n_3, and n_4 as indicated in Algorithm V.

APPENDIX B

Define $f(\tau;z,\gamma)=\tau\ln\left(1+\gamma\frac{z}{\tau}\right)$ with respect to τ for $0\le\tau\le 1$ and $g(\tau;z,\gamma)$ as $\frac{\partial f}{\partial\tau}=\ln\left(1+\frac{\gamma z}{\tau}\right)-\frac{\gamma z/\tau}{1+\gamma z/\tau}$. By calculating the first derivative of $g(\tau;z,\gamma)$ with respect to τ we get,

$$\frac{\partial g}{\partial\tau} = -\frac{z^2\gamma^2}{\left(\tau^3\left(1+\gamma z/\tau\right)^2\right)}\le 0. \quad (76)$$

Since $g(\tau;z,\gamma)$ is monotonically decreasing in τ in the interval $0\le\tau\le 1$, then, $\frac{\partial f}{\partial\tau}=\ln\left(1+\frac{\gamma z}{\tau}\right)-\frac{\gamma z/\tau}{1+\gamma z/\tau}\ge\ln\left(1+\gamma z\right)-\frac{\gamma z}{1+\gamma z}$.

Now, let us consider the function $P(x)=\ln(1+x)-\frac{x}{1+x}=\ln(1+x)+\frac{1}{x+1}-1$, where $x\in[0,\infty)$. This satisfies $P(0)=0$, $\lim_{x\to\infty}P(x)=\infty$, $P'(x^*)=\frac{x^*}{(x^*+1)^2}=0\Rightarrow x^*=0$ and $P''(x^*)=\frac{1-x^*}{(x^*+1)^3}\Rightarrow P''(0)=1>0$, which certifies that $x=0$ is a local minimum for $P(x)$.

Algorithm V

Input: $h_i, I_o, z_{\min}, \tau_{\min}, P_{\mathrm{M}}$
for $(n_1, n_2, n_3) \in \{0, \ldots, K\} \times \{0, \ldots, K-1\} \times \{0, \ldots, K-1\}$
  $n_4 \leftarrow K - n_1 - n_2 - n_3$
  if $0 \leq n_4 \leq K-1, n_1 + n_2 \geq 1, n_1 + n_3 \geq 1, n_1 > 0$
    Compute all the primal , and dual variables using equations (60) - (67)
  else if $0 \leq n_4 \leq K-1, n_1 + n_2 \geq 1, n_1 + n_3 \geq 1, n_1 = 0$
    Compute all the primal , and dual variables using equations (68) - (75)
  end if
  if $0 \leq n_4 \leq K-1, n_1 + n_2 \geq 1, n_1 + n_3 \geq 1$, primal and dual variables feasibility holds
    $\boldsymbol{z}_{\text{opt}} \leftarrow \boldsymbol{z}^*, \boldsymbol{\tau}_{\text{opt}} \leftarrow \boldsymbol{\tau}^*$
  end if
end for

Consequently, the global minimum of $P(x)$ for $x \in [0, \infty)$ is zero. Thus, $\ln(1+\gamma z) - \frac{\gamma z}{1+\gamma z} \geq 0$, which implies that $g(\tau; z, \gamma) \geq 0$ for $0 \leq \tau \leq 1$, which proves the positive monotonicity of $f(\tau; z, \gamma)$ for $0 \leq \tau \leq 1$ and $z \geq 0$.

APPENDIX C

For the considered configuration to be feasible, $\tau_j \geq \tau_{\min} \geq 0$ must hold, which implies that:

$$1 - \sum_{i=1}^{f-1} \tau_{\max,i} - (K-\ell)\,\tau_{\min} - \sum\nolimits_{i \in U_4} g_i(\lambda) \geq \tau_{\min} \geq 0. \tag{77}$$

By studying the monotonicity of $g_i(\lambda)$ we get:

$$g_i'(\lambda) = -z_{\min}\gamma_i \left(\mathcal{W}_0\left(-e^{-(\lambda+1)}\right) + 1\right)^{-2} e^{-(\lambda+1)} \leq 0. \tag{78}$$

For the two previous inequalities to hold $\lambda \leq \lambda_{\max}$ must be satisfied, where $\sum_{i \in U_4} g_i(\lambda_{\max}) = 1 - \sum_{i=1}^{f-1} \tau_{\max,i} - (K-\ell)\,\tau_{\min} - \tau_{\min}$.

To check the monotonicity of $G(\lambda)$, we differentiate (19) with respect to λ:

$$\frac{dG}{d\lambda} = \underbrace{\left(1 - \sum_{i=1}^{f-1} \tau_{\max,i} - (K-l)\,\tau_{\min} - \sum_{i \in U_4} g_i(\lambda)\right)}_{\geq 0 \text{ for } \lambda \leq \lambda_{\max}} \underbrace{\frac{e^{-\lambda-1}\mathcal{W}_0'\left(-e^{-(\lambda+1)}\right)}{\gamma_j \left(\mathcal{W}_0\left(-e^{-(\lambda+1)}\right)\right)^2}}_{\geq 0}$$
$$+ g_i'(\lambda) \underbrace{\left(\frac{1}{\gamma_j \mathcal{W}_0\left(-e^{-(\lambda+1)}\right)} + \frac{1}{\gamma_j}\right)}_{\leq 0} - \gamma_j \sum_{i \in U_2} \underbrace{f_i'\left(-\gamma_j \mathcal{W}_0\left(-e^{-(\lambda+1)}\right)\right)}_{\leq 0} \underbrace{\mathcal{W}_0'\left(-e^{-(\lambda+1)}\right) e^{-(\lambda+1)}}_{\geq 0} \tag{79}$$

Thus, by observing the signs of the factors in (68), we conclude that $\frac{dG}{d\lambda} \geq 0$ for $\lambda \leq \lambda_{\max}$.

REFERENCES

[1] A. M. Abdelhady, O. Amin, A. Chaaban, and M. S. Alouini, "Resource allocation for outdoor visible light communications with energy harvesting capabilities," in *IEEE Globecom Workshops (GC Wkshps)*, Singapore, Dec. 2017, pp. 1–6.

[2] M. A. Khalighi and M. Uysal, "Survey on free space optical communication: A communication theory perspective," *IEEE Commun. Surveys Tuts.*, vol. 16, no. 4, pp. 2231–2258, Jun. 2014.

[3] P. H. Pathak, X. Feng, P. Hu, and P. Mohapatra, "Visible light communication, networking, and sensing: A survey, potential and challenges," *IEEE Commun. Surveys Tuts.*, vol. 17, no. 4, pp. 2047–2077, Sep. 2015.

[4] D. Karunatilaka, F. Zafar, V. Kalavally, and R. Parthiban, "LED based indoor visible light communications: State of the art," *IEEE Commun. Surveys Tuts.*, vol. 17, no. 3, pp. 1649–1678, Mar. 2015.

[5] S. Wu, H. Wang, and C. Youn, "Visible light communications for 5G wireless networking systems: from fixed to mobile communications," *IEEE Network*, vol. 28, no. 6, pp. 41–45, Nov 2014.

[6] C.-X. Wang, F. Haider, X. Gao, X.-H. You, Y. Yang, D. Yuan, H. Aggoune, H. Haas, S. Fletcher, and E. Hepsaydir, "Cellular architecture and key technologies for 5G wireless communication networks," *IEEE Commun. Mag.*, vol. 52, no. 2, pp. 122–130, Feb. 2014.

[7] A. M. Abdelhady, O. Amin, A. Chaaban, and M.-S. Alouini, "Downlink resource allocation for multichannel TDMA visible light communications," in *Proc. IEEE Global Conf. Signal and Inform. Process. (GlobalSIP)*, Washington DC, 2016, pp. 1–5.

[8] A. M. Abdelhady, O. Amin, A. Chaaban, B. Shihada, and M.-S. Alouini, "Downlink resource allocation for dynamic tdma-based vlc systems," *IEEE Trans. Wireless Commun.*, vol. 18, no. 1, pp. 108–120, 2019.

[9] C. Gong, S. Li, Q. Gao, and Z. Xu, "Power and rate optimization for visible light communication system with lighting constraints," *IEEE Trans. Signal Process.*, vol. 63, no. 16, pp. 4245–4256, Aug. 2015.

[10] F. Jin, X. Li, R. Zhang, C. Dong, and L. Hanzo, "Resource allocation under delay-guarantee constraints for visible-light communication," *IEEE Access*, vol. 4, pp. 7301–7312, May 2016.

[11] D. Bykhovsky and S. Arnon, "Multiple access resource allocation in visible light communication systems," *J. Lightw. Technol.*, vol. 32, no. 8, pp. 1594–1600, Apr. 2014.

[12] X. Li, R. Zhang, and L. Hanzo, "Optimization of visible-light optical wireless systems: Network-centric versus user-centric designs," *IEEE Commun. Surveys Tuts.*, pp. 1–1, 2018.

[13] A. Căilean and M. Dimian, "Current challenges for visible light communications usage in vehicle applications: A survey," *IEEE Commun. Surveys Tuts.*, vol. 19, no. 4, pp. 2681–2703, Fourthquarter 2017.

[14] M. Uysal, Z. Ghassemlooy, A. Bekkali, A. Kadri, and H. Menouar, "Visible light communication for vehicular networking: performance study of a V2V system using a measured headlamp beam pattern model," *IEEE Veh. Technol. Mag.*, vol. 10, no. 4, pp. 45–53, Dec. 2015.

[15] I. Takai, T. Harada, M. Andoh, K. Yasutomi, K. Kagawa, and S. Kawahito, "Optical vehicle-to-vehicle communication system using LED transmitter and camera receiver," *IEEE Photon. J.*, vol. 6, no. 5, pp. 1–14, Oct. 2014.

[16] T. Rakia, H. C. Yang, F. Gebali, and M. S. Alouini, "Optimal design of dual-hop VLC/RF communication system with energy harvesting," *IEEE Commun. Lett.*, vol. 20, no. 10, pp. 1979–1982, Oct 2016.

[17] M. R. Zenaidi, Z. Rezki, M. Abdallah, K. A. Qaraqe, and M. S. Alouini, "Achievable rate-region of VLC/RF communications with an energy harvesting relay," in *IEEE Global Commun. Conf. (GLOBECOM)*, Dec. 2017, pp. 1–7.

[18] Y. Li, N. Huang, J. Wang, Z. Yang, and W. Xu, "Sum rate maximization for VLC systems with simultaneous wireless information and power transfer," *IEEE Photon. Technol. Lett.*, vol. 29, no. 6, Mar. 2017.

[19] Y. Liu, H. Y. Chen, K. Liang, C. W. Hsu, C. W. Chow, and C. H. Yeh, "Visible light communication using receivers of camera image sensor and solar cell," *IEEE Photon. J.*, vol. 8, no. 1, pp. 1–7, Feb. 2016.

[20] P. D. Diamantoulakis, G. K. Karagiannidis, and Z. Ding, "Simultaneous lightwave information and power transfer (SLIPT)," *IEEE Trans.Green Commun. Netw.*, Doi: 10.1109/TGCN.2018.2818325 2018.

[21] C. Zhang, J. Ye, G. Pan, and Z. Ding, "Cooperative hybrid VLC-RF systems with spatially random terminals," *IEEE Trans. Commun.*, vol. 66, no. 12, pp. 6396–6408, Dec. 2018.

[22] G. Pan, J. Ye, and Z. Ding, "Secure hybrid VLC-RF systems with light energy harvesting," *IEEE Trans. Commun.*, vol. 65, no. 10, pp. 4348–4359, Oct. 2017.

[23] G. Pan, H. Lei, Z. Ding, and Q. Ni, "On 3-D hybrid VLC-RF systems with light energy harvesting and OMA scheme over RF links," in *IEEE Global Commun. Conf. (GLOBECOM)*, Singapore, Dec. 2017, pp. 1–6.

[24] G. Pan, P. D. Diamantoulakis, Z. Ma, Z. Ding, and G. K. Karagiannidis, "Simultaneous Lightwave Information and Power Transfer: Policies, Techniques, and Future Directions," *IEEE Access*, vol. 7, pp. 28 250–28 257, Feb. 2019.

[25] J. M. Kahn and J. R. Barry, "Wireless infrared communications," *Proceedings of the IEEE*, vol. 85, no. 2, pp. 265–298, Feb 1997.

[26] A. Lapidoth, S. M. Moser, and M. Wigger, "On the capacity of free-space optical intensity channels," *IEEE Trans. Inf. Theory*, vol. 55, no. 10, pp. 4449–4461, Oct. 2009.

[27] R. Boylestad and L. Nashelsky, *Electronic devices and circuit theory 9th ed.* Pearson Education India, 2009.

[28] S. Boyd and L. Vandenberghe, *Convex optimization*. Cambridge university press, 2004.

[29] R. M. Corless, G. H. Gonnet, D. E. Hare, D. J. Jeffrey, and D. E. Knuth, "On the lambertw function," *Advances in Comput. Math.*, vol. 5, no. 1, pp. 329–359, 1996.

[30] K. R. Shailesh and T. Shailesh, "Review of photometric flicker metrics and measurement methods for LED lighting," in *2017 4th Int. Conf. on Adv. Comput. and Commun. Syst. (ICACCS)*, Coimbatore, India, Jan. 2017, pp. 1–7.